https://doi.org/10.1016/j.engstruct.2022.115293

Material properties and residual stresses of welded high strength steel and hybrid I-sections

Shuxian CHEN[1]; Jun-zhi LIU[2]; Tak-Ming CHAN[1]*

1 Department of Civil and Environmental Engineering, The Hong Kong Polytechnic University, Hong Kong, China

2 School of National Safety and Emergency Management, Beijing Normal University, China.

(Formerly, Department of Civil and Environmental Engineering, The Hong Kong Polytechnic University, Hong Kong, China)

* Corresponding author: tak-ming.chan@polyu.edu.hk

ZS931, Block Z, The Hong Kong Polytechnic University, Hung Hom, Hong Kong SAR

ABSTRACT:

High strength steel (HSS) I-sections are gaining increasing popularity compared with conventional strength steel counterparts, mainly due to its higher strength-to-weight ratio. Meanwhile, there has been growing interest in hybrid I-sections, which are made of different strength steels for flange and web plates, because of the increased need of maximising material utilization. This study investigates the welding effect on the material properties and residual stresses of welded HSS and hybrid I-sections. Tensile tests of coupons machined from both virgin plates and within the welded I-sections were carried out, followed by a metallographic analysis of welding position. It was found that the welding effect on the mechanical behaviour of steel materials varies, depending on the chemical composition and microstructure. Residual stress measurements for HSS and hybrid I-sections covering four web slenderness were conducted. The measurement results demonstrate that the effect of steel strength grade of constitutive plates on residual stress distribution of I-sections is negligible, and a new residual stress distribution model is proposed for welded HSS and hybrid I-sections examined in this study.

Keywords: Welding effect; Material property; Residual stress; High strength steel; Hybrid I-section.

1. Introduction

Because of the high strength-to-weight ratio, high strength steel (HSS) structures, with advantages of aesthetic, economical and environmental-friendly aspects, has gained increasing popularity. I-section (or H-section), a usual cross-section, has been widely used in steel columns and girders. Conceptualised firstly in 1944 [1], hybrid I-section, using different steel strength grades for flange and web plates, is expected to exploit the full potential of high strength steel and conventional strength steel. Studies have shown that hybrid I-beams exhibit better rotation capacity than HSS counterparts, which attributes to the greater material ductility of lower strength web [2-4]. The promising application prospect of HSS and hybrid I-sections draws researchers' attention these years [4-6]. In this study, HSS is defined as the steel with nominal yield strength $f_{y,nom}$ greater than 460 N/mm^2 [7].

To account for diverse needs of cross-section dimension and material combination, welding becomes a prevailing manufacturing method for I-sections. Nevertheless, the high temperature produced by welding process induces the transformation in the microstructure of steel materials, as well as the internal stress within sections because of local thermal expansion and contraction [8]. Moreover, steel production techniques, such as quenching and tempering (QT) process, and thermomechanical controlled (TMCP) process, affect the mechanical behaviour of steel material near the welding seam [9]. Though material properties of HSS virgin plates have been extensively studied [10–16], and numerous experimental investigations about the welding effect on the material properties of HSS and hybrid sections featured with hollow profile [7,17–20] have been performed, the effect of manufacturing process and production techniques on HSS and hybrid I-sections have not been closely examined.

The significance of welding-induced residual stresses on the structural behaviour is well-recognised. A well understanding of residual stress distribution within cross-sections helps facilitate the structural performance design, as well as the numerical analysis. In the last decade, Wang et al. [21] measured the residual stresses of flame-cut Q460 H-sections ($f_{y,nom}$ = 460 N/mm^2) by sectioning method and hole-drilled method, both of which were found to present similar results of residual stress distribution. The residual stress tests for welded Q690 H-sections ($f_{y,nom}$ = 690 N/mm^2) were also carried out by Li et al. [22]. The same distribution pattern as Wang et al.'s model [10] but with different magnitudes was established. Yang et al. [23-24] investigated the residual stress distribution model for Q460GJ doubly and singly symmetric medium and thick-walled I-shaped sections ($f_{y,nom}$ = 460 N/mm^2), and it was concluded that greater residual stresses exist in thin plates than thicker ones. Liu and Chung [25-26] explored the surface temperature histories and internal residual stress of welded S690 H-sections ($f_{y,nom}$ = 690 N/mm^2) by experiments and numerical methods; a simplified model taking account of heat input energy and plate thickness was proposed. Recently, non-destructive neutron diffraction method was utilised by Li et al. [27] to measure the residual stresses of box and I-shaped S960 ($f_{y,nom}$ = 960 N/mm^2) sections, and simplified residual stress predictive equations incorporating the plate thickness was established. The applicability of the residual stress predictive models in the aforementioned literatures is conditional, due to the limited coverage in terms of dimensions and steel materials of test specimens. Ban [28] established a unified residual stress pattern for I-sections underpinned by the measurement results of Q460 ($f_{y,nom}$ = 460 N/mm^2) and Q960 ($f_{y,nom}$ = 960 N/mm^2) test specimens and a statistical analysis of existing data from other papers. Ban's model concentrates on the homogenous I-sections, for which the same steel strength is used for flange and web plates.

Existing data on the residual stresses of hybrid I-sections is limited. The earliest investigation concerning hybrid sections can be traced back to Frost and Schilling [29] who measured residual stresses of three I-sections with identical nominal dimensions but different strength web. Afterwards, Nagarajarao et al. [30] undertaken the residual stress measurement for five hybrid I-sections. Both above-mentioned measurement results argued that residual stress distribution of hybrid I-sections are basically similar to the homogeneous ones. The most recent research is the experimental studies of residual stress at the University of Coimbra and Ruhr-Universität Bochum, reported by Schaper et al. [31]. Two hybrid I-sections were involved in that research, and a new residual stress model applicable to I-sections was suggested. To date, only a limited number of residual stresses for hybrid I-sections have been identified.

In addition, most of the current design recommendations of residual stress pattern for welded I-sections are characterised with the tensile residual stress at the weldment $f_{r,ft}$ equalling the material yield strength f_y [32-34], whereas measurement results on HSS and hybrid I-sections reported in the literature indicate that no evident correlation was observed between $f_{r,ft}$ and f_y, with the ratio of $f_{r,ft}$ to f_y varying from 0.28 to 1.0 [21-28]. An experimental comparison between HSS and hybrid I-sections helps understand the effect of steel strength grade on the magnitude of welding-induced tensile residual stress.

This study therefore focuses on the welding effect on the material properties and residual stresses of HSS and hybrid I-sections. A total of twelve test specimens covering four web slenderness, consisting of eight hybrid-sections and the homogenous counterparts, were studied. Tensile coupon tests for both virgin plates and welded I-sections were carried out, followed by a metallographic analysis to further explore the differences among different strength webs. Residual stress measurements were executed for all the specimens by sectioning method, and a comparison between the measurement results and existing models is discussed. A residual stress distribution predictive model applicable to I-sections in this study is proposed.

2. Test Specimens

Twelve I-section test specimens, with nominal geometrical characteristics presented in Table 1, were tested to examine the welding effect on the material properties and residual stresses of welded I-sections. In Figure 1, b_f and t_f are the flange width and flange thickness respectively; H and h_w represent the section height and clear distance between flanges; t_w is the thickness of web plate. Four web slenderness (h_w/t_w) of 35, 49, 55 and 70 were covered.

Table 1. Nominal geometrical characteristics of welded I-section test specimens

Specimens	b_f (mm)	t_f (mm)	h_w (mm)	H (mm)	t_w (mm)	b_f/t_f	h_w/t_w
H230-Q690	110	10	210	230	6	11	35
H230-Q460							
H230-Q355							
H310-Q690			290	310			49
H310-Q460							
H310-Q355							
H350-Q690			330	350			55
H350-Q460							
H350-Q355							
H440-Q690			420	440			70
H440-Q460							
H440-Q355							

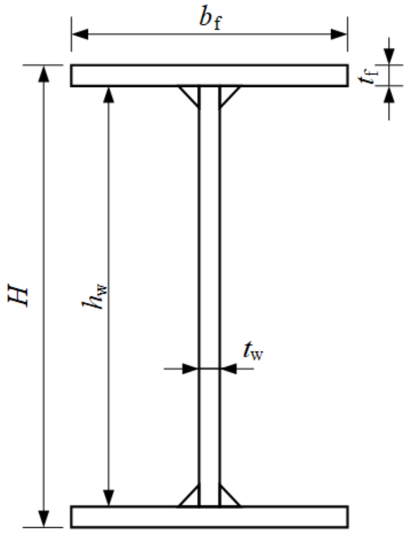

Figure 1. I-shaped cross-section

All flanges were made of 10 mm thick Q690 steel, while three grades of 6 mm thick steel plates - Q690, Q460 and Q355 were used as the web plates. The nomenclature of specimens in Table 1 is interrelated to the section height and the web grade, for example, “H350-Q460” represent a specimen with 350 mm section height and fabricated by Q460 web plate. The chemical composition of four virgin plates (wt%) is summarisd in Table 2, where, “Q690-F” is the plate employed for flange, “Q690-W”, “Q460-W” and “Q355-W” are those for web plates. It is noted from this table that compared with other steel materials, the carbon (C) and silicon (Si) contents of “Q460-W” are much less, while its micro-alloying elements-Niobium (Nb) and Nickel (Ni) are higher. In this table, CEV is carbon equivalent value, calculated by

$$\mathrm{CEV}=\mathrm{C}+\mathrm{Mn}/6+(\mathrm{Cr}+\mathrm{V}+\mathrm{Mo})/5+(\mathrm{Cu}+\mathrm{Ni})/15 \tag{1}$$

Table 2. Chemical composition of virgin plates (wt %)

Steel plates	C	Si	Mn	P	S	Nb	Ti	Cr	Mo	B	V	Cu	Ni	Al_t	N	CEV
Q690-F	0.13	0.30	1.04	0.014	0.0015	0.022	0.018	0.34	0.23	0.0022	0.042	0.03	0.01	0.034	/	0.43
Q690-W	0.14	0.27	1.40	0.019	0.001	0.024	0.013	0.26	0.14	0.0015	/	/	/	/	/	0.46
Q460-W	0.07	0.16	1.59	0.012	0.002	0.055	0.011	0.04	0.17	0.0003	0.02	0.03	0.17	0.030	/	0.39
Q355-W	0.14	0.26	1.29	0.016	0.001	0.013	0.015	0.08	0.003	/	0.002	0.02	0.03	0.035	0.0046	0.38

By the means of gas metal arc welding (GMAW) with mixture of 80% Argon (Ar) and 20% carbon dioxide (CO_2), 6 mm fillet welds were used to connect the flanges and web. The selection of weld metal was in accordance with the mechanical properties of web plate to avoid the occurrence of cold cracking [35-36]. The welding wires corresponding to I-sections made of Q690, Q460 and Q355 web plates were “ER69-G”, “ER55-Ni mod” and “ER50-6”, respectively [37]. The chemical composition of welding wires is shown in Table 3. The welding process was executed manually by a skilled technician, and the welding voltage U was 31~32 V; the welding current I was 230~240 A; the welding speed υ was 4.5~4.6 mm/s. By Equation (2), as the arc efficiency η of GMAW is taken as 0.85 [8], the welding heat input Q is about 1.38 KJ/mm.

$$Q = \frac{\eta \times U \times I}{v} \tag{2}$$

Table 3. Chemical composition of welding wires (wt%)

Welding wires	C	Si	Mn	P	S	Cr	Mo	Ni	V	Cu	Al	Ti
ER69-G	0.09	0.65	1.62	0.010	0.010	0.17	0.47	1.46	0.006	0.10	0.004	0.05
ER55-Ni mod	0.09	0.73	1.42	0.007	0.001	0.050	0.004	1.36	0.001	0.070	0.012	/
ER50-6	0.07	0.86	1.5	0.016	0.010	0.04	0.001	0.03	0.001	0.10	/	/

3. Material tests

3.1. Tensile coupon tests

3.1.1. Virgin plates

Six tensile coupons were cut from each virgin plate, among which three were parallel to the rolling direction and the others were perpendicular to the rolling direction. The dimensions of coupons were determined in accordance with ISO 6892-1 [38], as shown in Figure 2. Material tests were conducted by using a 100 kN electromechnical universal testing machine (UTM) with the advanced video extensometer (AVE) in the Industrial Centre at The Hong Kong Polytechnic University (Figure 3). The measured full stress f-strain ε curves of coupons cut from virgin plates are displayed in Figure 4, and the average measured material characteristics are presented in Table 4. In this table, E is the elastic modulus; ε_y, ε_{sh} and ε_u represent the yield strain, strain at the onset of strain hardening and ultimate strain; f_u refers to the ultimate strength. It is apparent from the figure and table, all the steel materials from the virgin plates possess the well-defined yield strength.

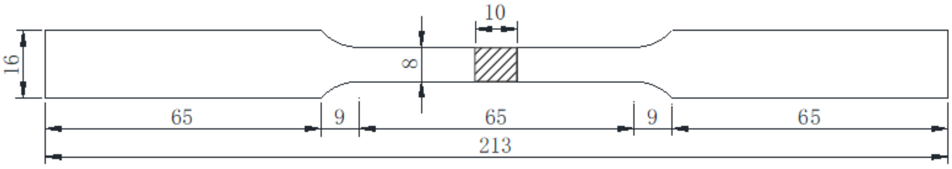

(a) Flange

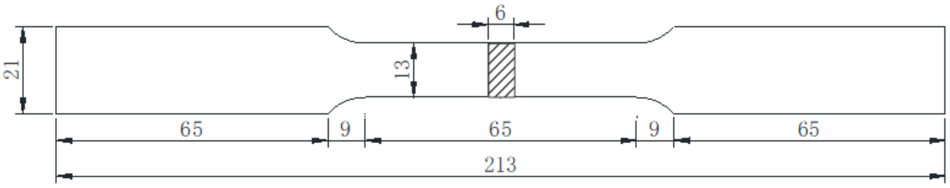

(b) Web

Figure 2. Dimensions of coupons cut from virgin plates

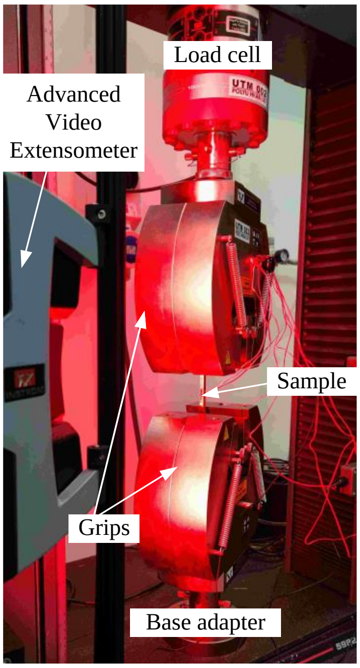

Figure 3. Setup of tensile coupon tests

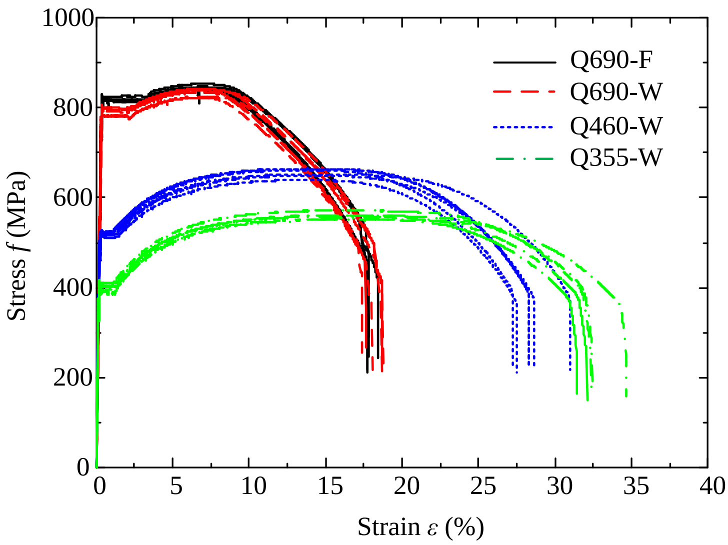

Figure 4. Full stress-strain curves of coupons cut from virgin plates

Table 4. Average measured material properties of steel materials

Steel plates	E (GPa)	ε_y (%)	ε_{sh} (%)	ε_u (%)	f_y (MPa)	f_u (MPa)
Q690-F	216.2	0.378	3.44	6.78	817.7	846.1
Q690-W	217.2	0.363	2.42	6.92	788.6	834.5
Q460-W	215.2	0.240	1.27	13.9	517.4	655.3
Q355-W	217.4	0.181	1.31	16.2	394.1	559.6

3.1.2 Welded I-sections

To evaluate the influence of welding heat input on the material properties of welded I-sections, material tests for a total of 96 coupons machined from constitutive plates of test specimens were carried out. The position of coupons is shown in Figure 5. In this figure, “WF” and “WW” represent the samples waterjet-cut from flanges and webs, respectively; the labels “1, 2, 3, 4” indicate its distance to the weldment. The centreline of “WF1”, “WF2”, “WF3” and “WF4” is 5 mm, 11 mm, 17 mm and 23 mm to the edge of weldment, and the distance from the centreline of “WW1”, “WW2”, “WW3” and “WW4” to the edge of weldment is 6 mm, 14 mm, 22 mm, 30 mm. According to ISO 6892-1 [38], the dimensions of “WF” and “WW” were designed as shown in Figure 6.

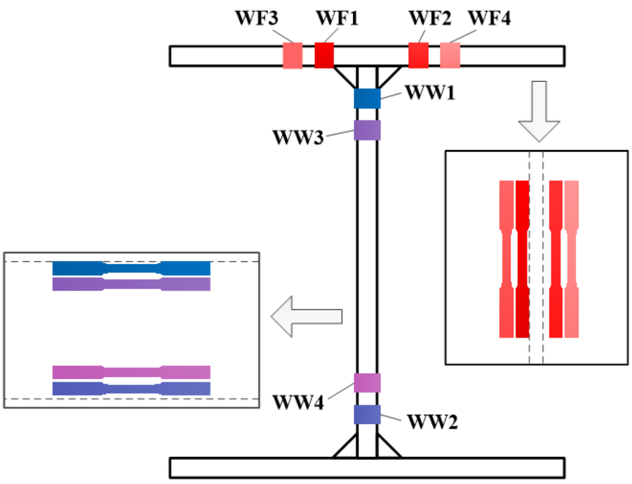

Figure 5. Position of coupons machined from welded I-sections

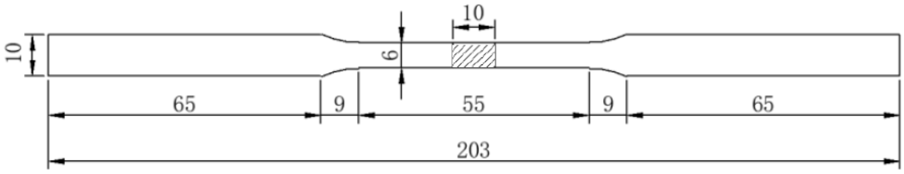

(a) Flange

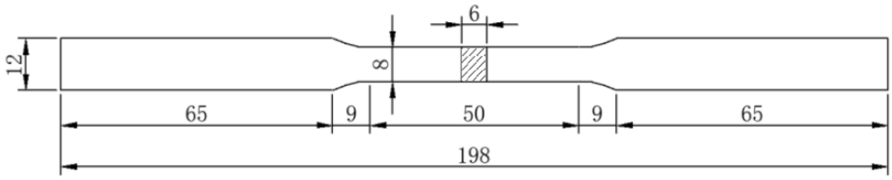

(b) Web

Figure 6. Dimensions of coupons machined from constitutive plates of welded I-sections

Figures 7 and 8 provide the tensile test results of coupons from welded I-sections. For the purpose of comparison, their yield strength f_y, tensile strength f_u, and yield-to-tensile ratio f_y/f_u are normalised by material properties of the corresponding virgin plates. For samples from the flange plates of welded I-sections, the normalised material characteristics are between 0.95 and 1.05. The normalised tensile strength f_u, yield strength f_y and yield-to-tensile f_y/f_u is lesser if it is closer to the weldment. The results from welded I-sections with Q460 web are selected to be representative, shown in Figure 7.

Likewise, same phenomenon on the tensile strength f_u was also observed in the material test results of coupons from the web plates. It worth mentioning that a distinction was identified among the tensile test results (normalised f_y and f_y/f_u) of coupons from the webs of welded I-sections. In Figure 8(a), ranging from 0.95 to 1.05, both the normalised yield strength f_y and yield-to-tensile f_y/f_u of coupons cut from specimens with Q690 web rise as the distance from the weldment increase. A similar trend was observed in the material tests of coupons from Q355 webs of I-sections (Figure 8(c)), of which the variation is greater, i.e., from 0.85 to 1.10. In contrast, what stands out in Figure 8(b) is the opposite tendency for the normalised yield strength f_y and yield-to-tensile ratio f_y/f_u was observed for web plates of specimens made of Q460 steel. Further explanation will be in given by the metallographic analysis in Section 3.2.

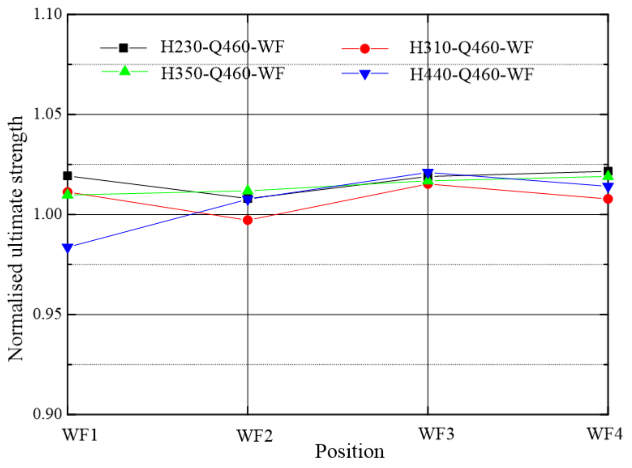

(a) Normalised ultimate strength

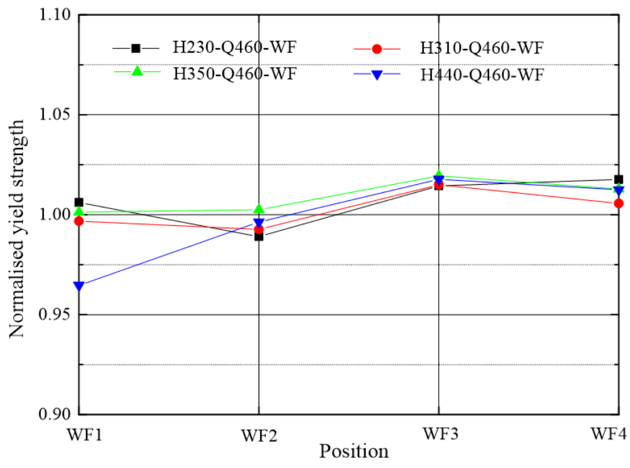

(b) Normalised yield strength

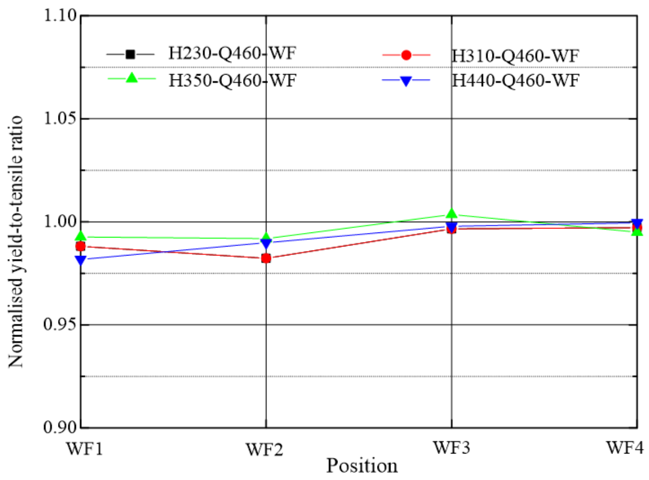

(c) Normalised yield-to-tensile ratio

Figure 7. Tensile test results of coupons from the flange plates of welded I-sections with Q460 web

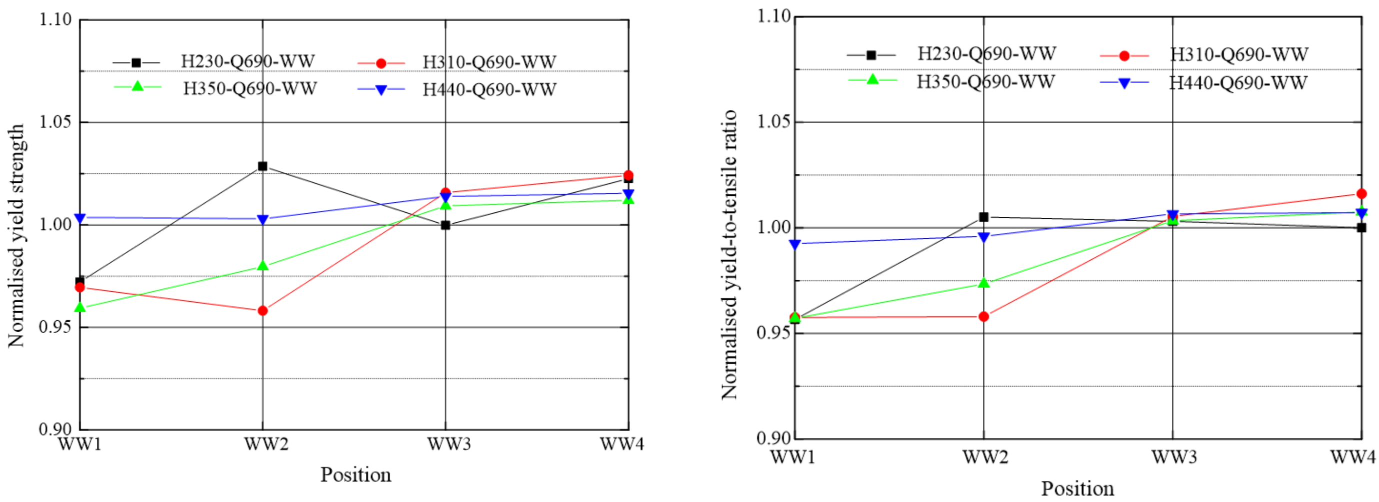

(a) I-sections with Q690 web

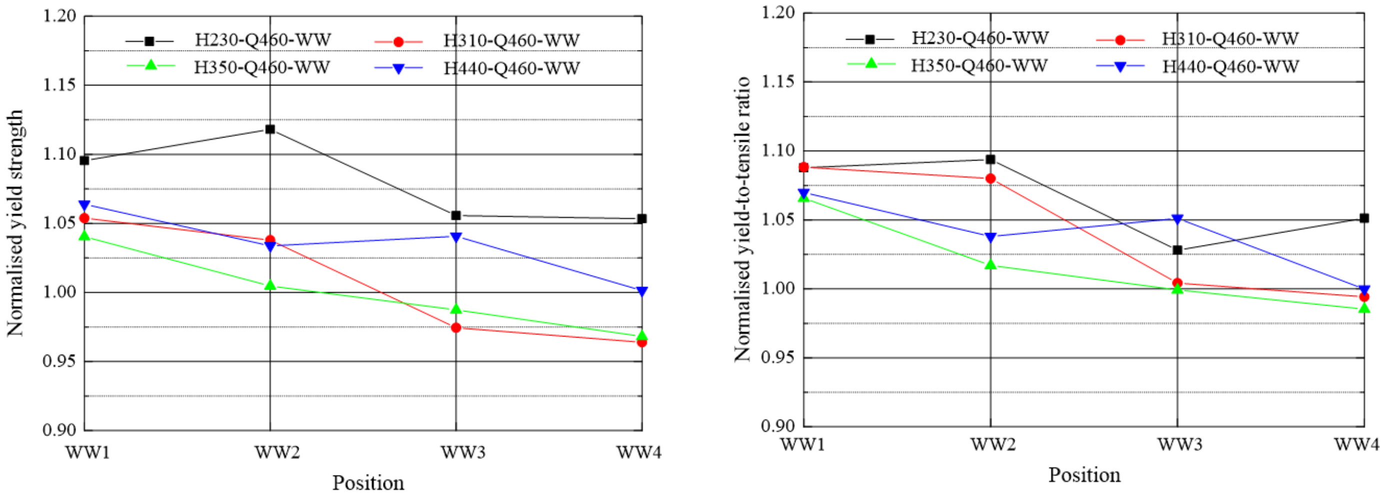

(b) I-sections with Q460 web

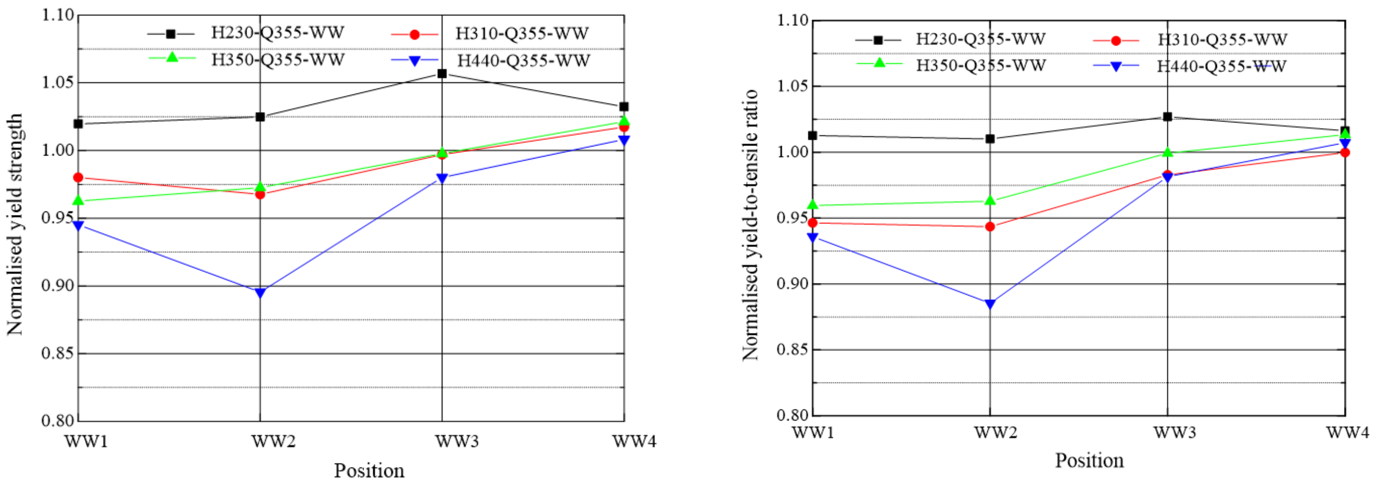

(c) I-sections with Q355 web

Figure 8. Normalised yield strength and yield-to-tensile ratio of coupons from the web plates of I-sections

To examine the dissimilarity of the mechanical behaviour among specimens with different web steel grades, the full stress-strain curves of web coupons from “H310-Q690”, “H310-Q460” and “H350-Q355” were shown in Figure 9. For specimens made of Q690 and Q355 steels (Figures 9(a) and 9(c)), the coupons closer to weldment (WW1 and WW2) show no distinct yield plateau, but characterised by the round material response. By contrast, WW1 and WW2 corresponding to the I-sections with Q460 web (Figure 9(b)) still possess a well-defined yield point, but there has been a slight decrease in the yield strength f_y and length of yield plateau in comparison with WW3 and WW4.

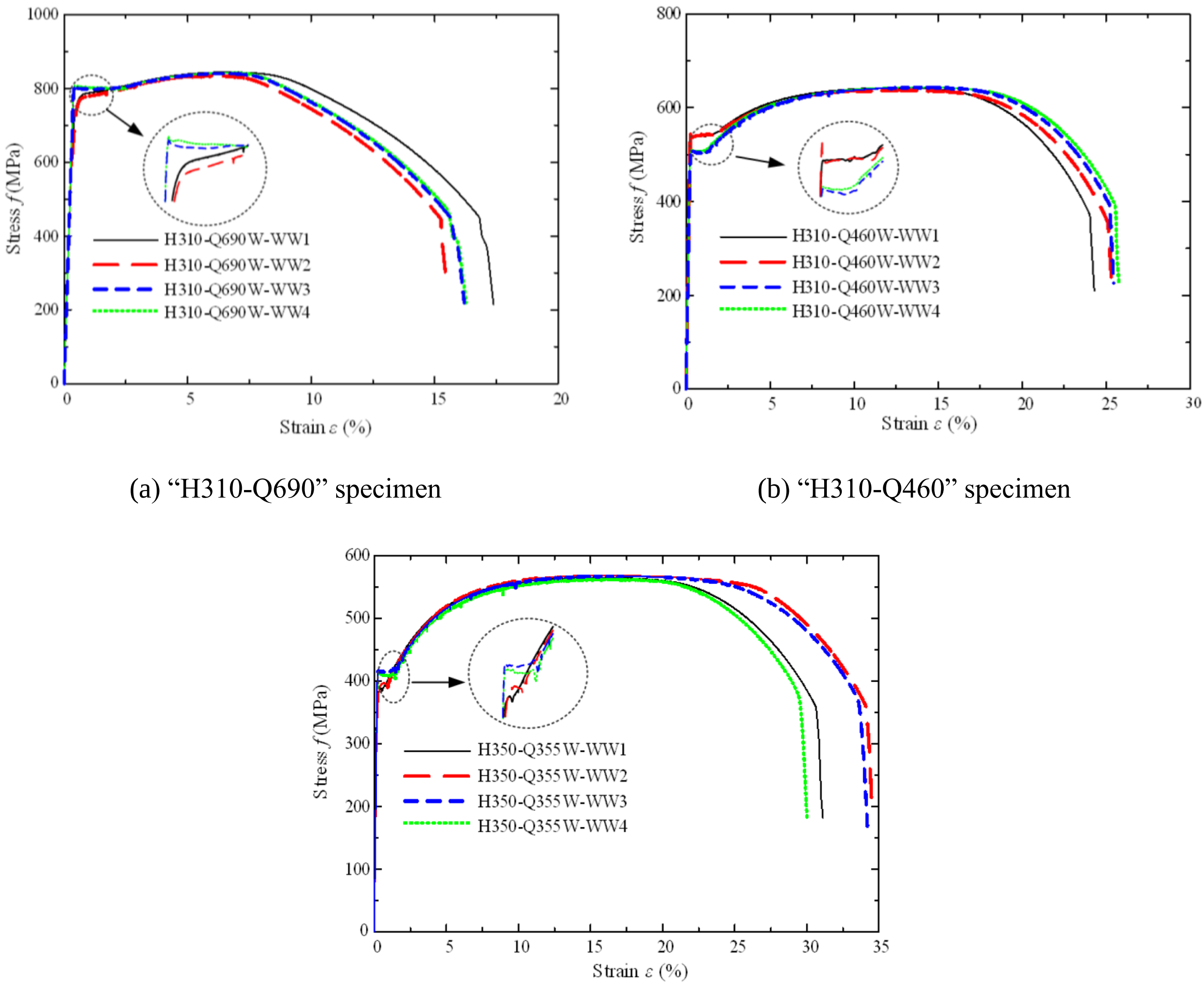

(a) “H310-Q690” specimen

(b) “H310-Q460” specimen

(c) “H350-Q355” specimen

Figure 9. Full stress-strain curves from coupon test results from the web plate of welded I-sections

3.2. Metallographic Analysis

To examine distinct material test results observed from samples of welded I-sections with Q460 web steel, metallographic examination was conducted in the Industrial Centre at The Hong Kong Polytechnic University. Metallographic specimens were sectioned from welding position of welded I-sections, and then mounted using a mixture of epoxy resin adhesive and epoxy resin curing agent. After that, the specimens were grounded by "Buehler EcoMet 30" equipped with 180, 320, 400, 600, 1000, 1200 and 2000 grit SiC grinding papers, followed by the mechanical polishing lubricated with 3μm polycrystalline diamond suspension. Lastly, the properly polished specimens were etched by 4% Nitric acid alcohol etchant for one minute for highlighting the microstructural features. The industrial inspection microscope ICM-100 with 3MP Camera US300 was chosen to observe the microstructure of metallographic specimens. Main procedures of metallographic examination are set out in Figure 10.

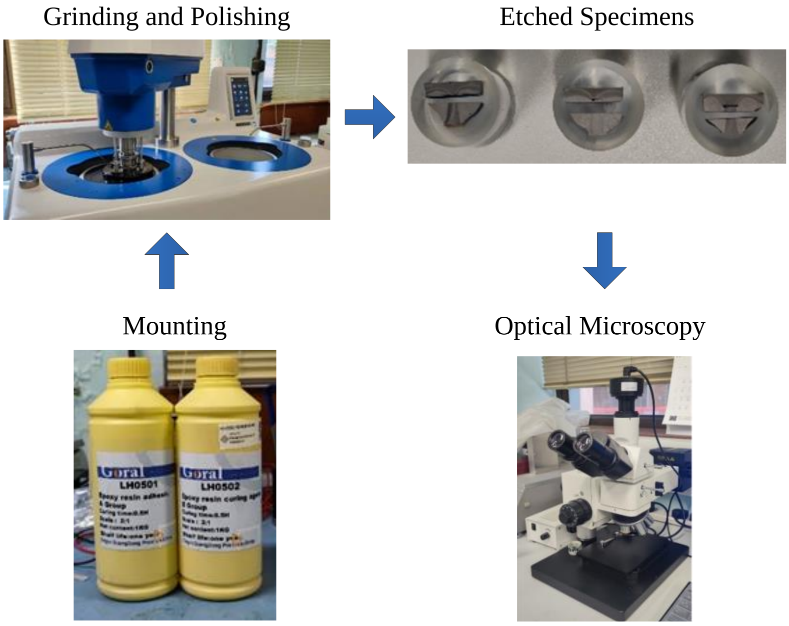

Figure 10. Main procedures of metallographic examination

Figure 11 presents the optical microstructure of base metal for web plates. Tempered martensite is distinguished from Q690 web plate, and Q355 steel contains ferrite and pearlite, while the micrograph of Q460 steel consists of granular bainite, pearlite and ferrite, which is a typical microstructure of low carbon bainitic steel. This observation is consistent with the chemical composition of Q460 virgin plate, as shown in Table 2: the content of C is 0.07, much lower than other steels in this study, with high-content micro-alloying additives, i.e., 0.055Nb and 0.17Ni (wt%).

Specially, the optical microstructure of coarse-grain heat-affected zone (CGHAZ) for one specimen made of

Q460 web is displayed in Figure 12. Figure 12(a) is the CGHAZ near the flange, characterised by parallel lath martensite, whereas granular bainite is identified for the CGHAZ near the web in Figure 12(b). This finding reveals that the distinct microstructures may form for different base metals even if under the same welding condition [39].

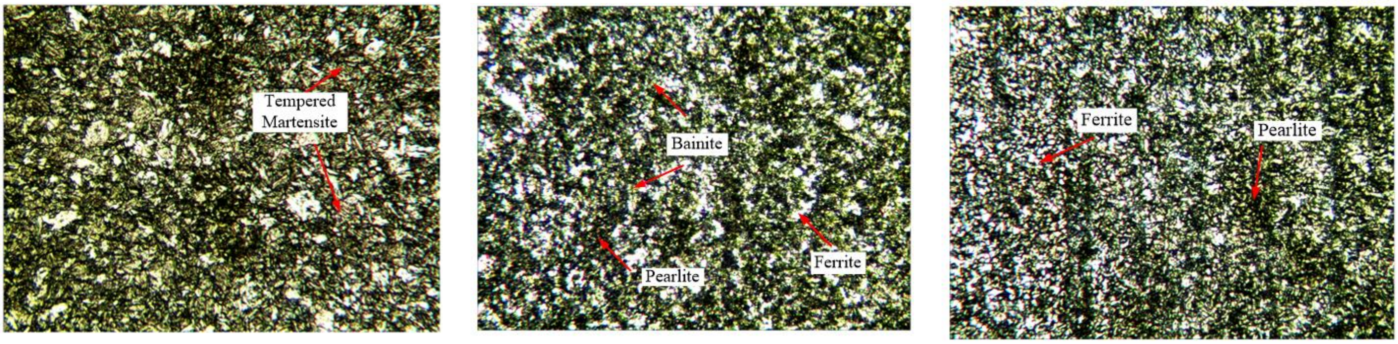

(a) Q690 web (b) Q460 Web (c) Q355 Web

Figure 11. Optical microstructure of base metal for web plates (magnitude: ×200)

(a) near the flange (b) near the web

Figure 12. Optical microstructure of coarse-grain heat-affected zone (CGHAZ) of welded I-sections with Q460 web (magnitude: ×500)

In addition, the phenomenon on the mechanical behaviour of coupons from Q460 web plates, as stated in Section 3.1.2, could be explained by its chemical composition and microstructure. It is generally true that during the welding process, high temperature resulting from heat input would decrease the high-density dislocation within coupons, and thus lower the steel yield strength f_y. But for low carbon bainitic steels, e.g., Q460 in this study, the precipitation strengthening from micro-alloying carbides enhances the yield strength of coupons near the weldment, which outstrips the detrimental effect of decreased dislocation density [40-42]. This phenomenon is similar to the findings in papers concerning about the effect of tempering temperature on the mechanical properties of 690 MPa Grade low carbon bainitic steels [43-44], that the increase of tempering temperature would rise up the steel yield strength.

4. Membrane residual stress measurement

4.1. Measurement method

To find out the residual stress distribution of HSS and hybrid I-sections, the stress-relieved sectioning method was adopted. Test specimens were firstly divided into strips by visible marks, and the strain gauges were then attached onto the mid-position of each strip on both sides, protected by the moisture- and water-proofing butyl rubber SB tape coating. Prior to sectioning, the initial readings of strain gauges were recorded to exclude the effect of adhesive pressure. The precise wire-cutting process for sectioning I-sections into strips was conducted along with the ongoing coolant to minimise the heat input. After complete sectioning, the strain gauge readings of each strip were recorded again to capture the strain variation because of stress relieving. The whole measurement process was carried out in a laboratory with strictly controlled temperature and humidity, and the strains of each cut strip after completing sectioning were measured by reconnecting to the same channel of data logger as the initial recordings obtained before cutting. The strain readings of each strip were recorded three times to get an average value by reconnecting to the data logger, and each recording was performed after 1-2 mins when the data becomes stable. In addition, the impact of the temperature, humidity, and electric resistance on strain variations was conducted by affixing the strain gauges to the virgin plate with measuring procedures analogous to the tested strips. It was of worthy noted that about 10 - 20 $\mu\varepsilon$ strain variations were obtained, primarily due to the essential errors from the environmental and instrumental effects, which are minimal and negligible. Similar measurement procedures were also utilised by other researchers [45-49].

The arrangement of strips for each I-section dimension is shown in Figure 13, where red dash lines indicate the reference lines for wire-cutting. The strip width was 9 or 10 mm for flange plates and the web part near the weldment. As previous research [21-24, 28-31] have shown that there is only a minor variation in the magnitude of membrane residual stress near the middle of the web in I-section, the width of strips close to web central line was selected to be wider -15 mm.

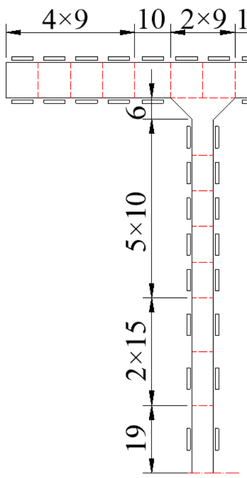

(a) “H230” specimens

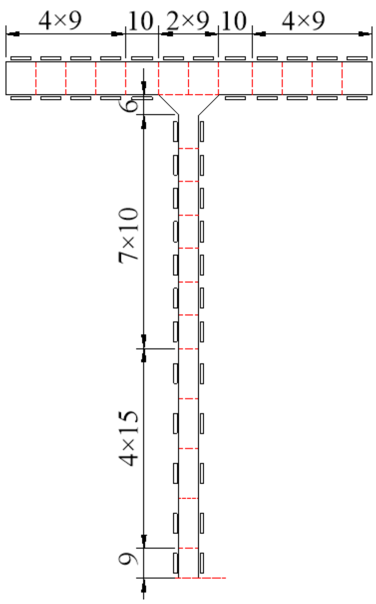

(b) “H310” specimens

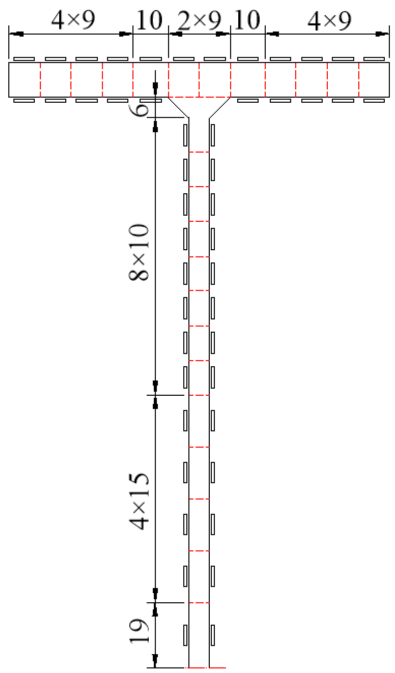

(c) “H350” specimens

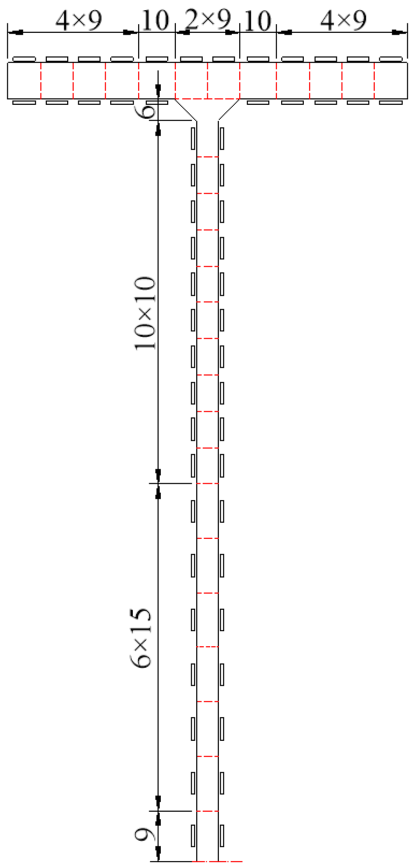

(d) “H440” specimens

Figure 13. Arrangement of wire-cut strips for residual stress measurement

The sectioning process of test specimens is illustrated by Figure 14. The membrane residual stress σ_{m} for each strip is calculated by Equations (3) and (4) [19].

$$\varepsilon_{\mathrm{o}} = \varepsilon_{\mathrm{o}}^{\mathrm{a}} - \varepsilon_{\mathrm{o}}^{\mathrm{b}};\ \varepsilon_{\mathrm{i}} = \varepsilon_{\mathrm{i}}^{\mathrm{a}} - \varepsilon_{\mathrm{i}}^{\mathrm{b}} \tag{3}$$

$$\sigma_{\mathrm{m}} = -E\left(\varepsilon_{\mathrm{o}} + \varepsilon_{\mathrm{i}}\right)/2 \tag{4}$$

where, $\varepsilon_{\mathrm{o}}^{\mathrm{a}}$ and $\varepsilon_{\mathrm{o}}^{\mathrm{b}}$ denote the strain recorded for the outer surface of the strip after and before sectioning; $\varepsilon_{\mathrm{i}}^{\mathrm{a}}$ and $\varepsilon_{\mathrm{i}}^{\mathrm{b}}$ are the ones measured for the inner surface after and before sectioning; ε_{o} and ε_{i} represent the strain variation of outer and inner surfaces, respectively. Based on the assumption of symmetry, one-half of web plates were involved in the residual stress measurement.

Figure 14. Sectioning of I-section test specimens for residual stress measurement

4.2. Measurement results

It has been well known that the internal residual stress arises from local heat input within sections. The constitutive plates of I-sections in this study were produced by thermal-based plasma-cutting process, of which the ionized gas reach a temperature of up to 25000 °C [50], tensile internal stress thus has existed at the tips of the flange and web plates before welding. During the welding process, the heat of fillet welding in the middle of flanges and at the edge of webs undoubtedly brings about high tensile residual stress at the location of weldment, balanced by the compressive stresses forms in the remainder part.

The residual stress measurement results of twelve welded I-sections are shown in Figure 15. In Figure 15, $f_{r,f}$ and $f_{r,w}$ represent the residual stress measured for flange pate and web plate respectively; the positive and negative numbers mean the tensile and compressive residual stresses respectively. As can be seen from these figures, specimens with identical nominal dimensions, but different web steels generally show similar distribution pattern, which shows agreement with the observations of Frost and Schilling [29] as well as Nagarajarao et al. [30]. In addition, for the compressive residual stresses at the web, uniform distribution was observed in the I-sections with 230 mm section height in Figure 15(a). But for specimens with slenderer web, i.e., “H310”, “H350” and “H440” series, gradually decreased compressive residual stresses were detected, even nearly equalling to zero when approaching the centre of web, as presented by Figures 15(b)~(d). A possible explanation for this might be that these heights of web are high enough to balance the tensile stresses caused by welding. Figure 16 shows the normalised closing error by the steel yield strength f_y for self-equilirbum of each plate. It was revealed that self-equilirbum of internal residual stress for each individual plate can be realised, with maximum normalised value equalling to 3.8%, which is acceptable in the engineering field.

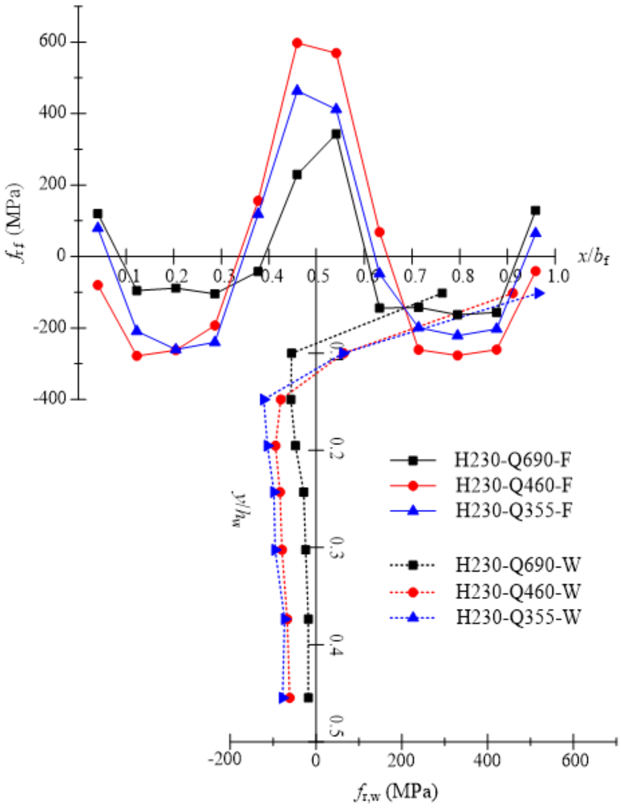

(a) “H230” specimens

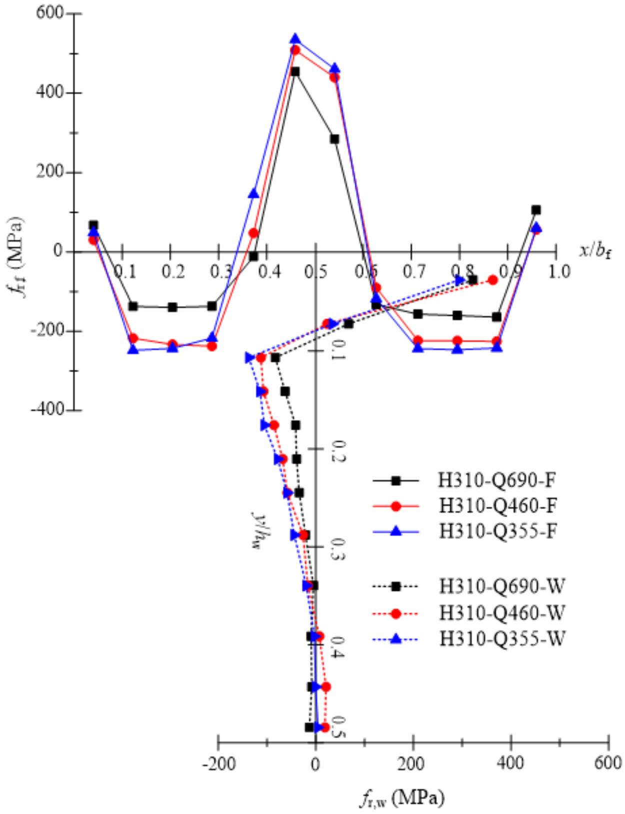

(b) “H310” specimens

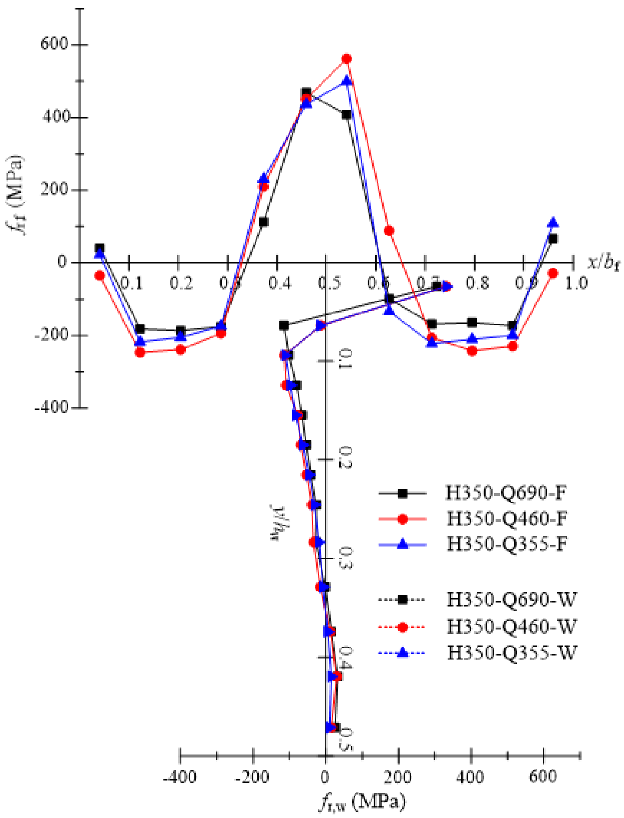

(c) “H350” specimens

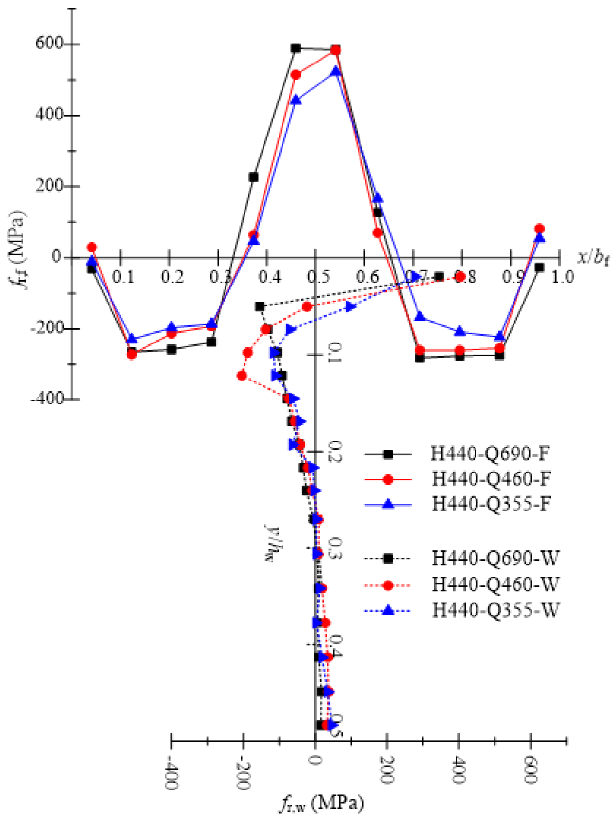

(d) “H440” specimens

Figure 15. Membrane residual stress measurement results of welded I-sections

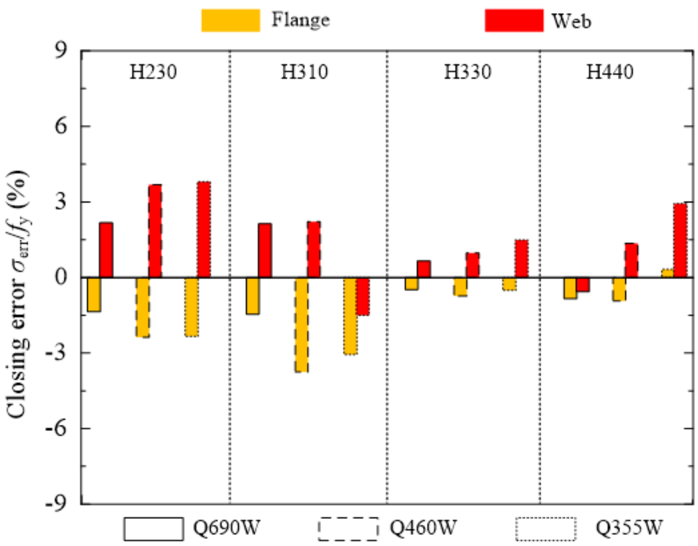

Figure 16. Normalised closing error for each individual plate of welded HSS and hybrid I-sections

4.3. Existing residual stress distribution models

As stated in the introduction, Ban [28] and Schaper et al. [31] individually established the unified residual stress distribution models for HSS H or I-sections, which are set out in Figure 17 and Table 5. In Figure 17, h_f is the width of fillet weld; $f_{r,wt}$ is the tensile residual stress for web at the location of weld; $f_{r,fte}$ represent the residual stress at the flange tips; $f_{r,fc}$ and $f_{r,wc}$ denote the compressive stresses at the flange and web, respectively. The meanings of $b_{r,i}$ (i = 1~5) and $h_{r,i}$ (i =1~2) in Table 5 are illustrated in Figure 17. It is indicated in this table that Ban's model adopts constant values for the tensile residual stresses, whilst $\sqrt{235/f_y}$ is defined in Schaper's model to consider the influence of steel strength grade. Another main difference between them is that only rectangular stress blocks are in Schaper's model, while Ban [28] uses triangle shapes to take the transition of tensile and compressive stresses into account. It should be noted that there has been two hybrid I-sections in Schaper's dataset.

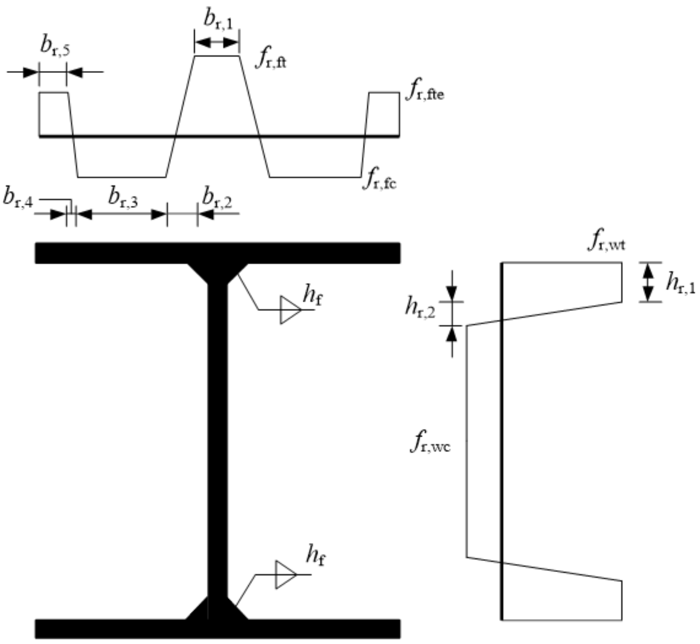

Figure 17. Diagram of existing unified residual stress distribution model

Table 5. Existing unified residual stress distribution models

Literatures	Ban [28]	Schaper et al. [31]
$f_{r,ft}/f_y$	$345/f_y$ # or $460/f_y$ *	$\sqrt{235/f_y}$
$f_{r,fc}/f_y$	Equation	Equilibrium
$f_{r,fte}/f_y$	$50/f_y$	$0.5\times\sqrt{235/f_y}$
$f_{r,wt}/f_y$	$345/f_y$ # or $460/f_y$ *	$\sqrt{235/f_y}$
$f_{r,wc}/f_y$	Equation	Equilibrium
$b_{r,1}/b_f$	$(t_w+2h_f)/b_f$	$\min\{t_w+5h_f; b_f/5\}$
$b_{r,2}/b_f$	Equilibrium	0
$b_{r,3}/b_f$	Equilibrium	Equilibrium
$b_{r,4}/b_f$	$0.1(b_f-h_f)$	0
$b_{r,5}/b_f$	$0.1(b_f-h_f)$	1/16
$h_{r,1}/h_w$	h_f/h_w	0.1
$h_{r,2}/h_w$	Equilibrium	0

Note: # means the value is applicable to steels with $f_{y,nom}$ between 345 and 550 N/mm^2; * means the value is applicable to steels with $f_{y,nom}$ greater than 550 N/mm^2.

Both of the above two models were compared with meausrement results in this study. Figure 18 presents the comparison results for flange plates. It can be said that these two models are able to generally predict the residual stress distribution of flanges for test specimens, whilst Schaper's model overestimates the tensile residual stress at the flange tips.

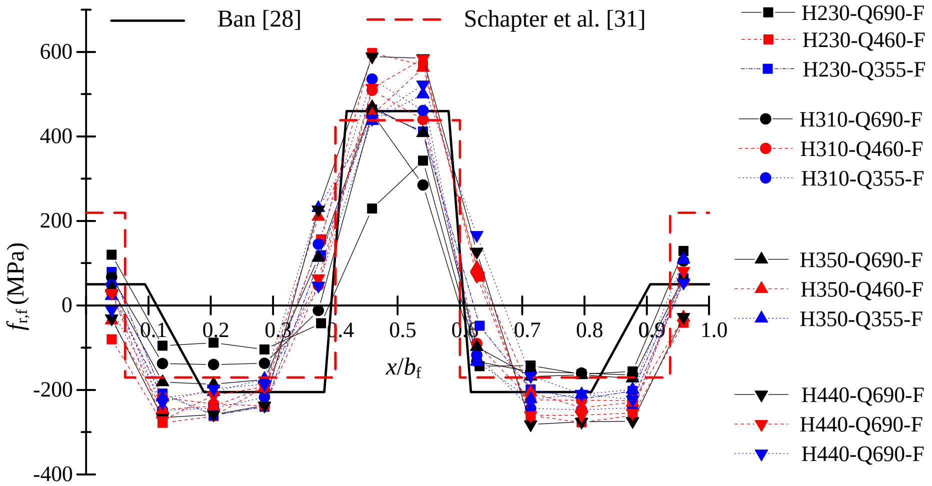

Figure 18. Comparison of existing unified distribution models and residual stress measurement results for flange plates of welded I-sections

The comparison of Ban's model and the measurement results for web plates is shown in Figure 19. It is apparent that Ban's model overestimates the range of transition between tension and compression zone. In comparison, the estimation for the range of web tensile and compressive zones of Schaper's model is more accurate for specimens, as shown in Figure 20. Regarding the compressive residual stresses of webs, both models overpredict measurement results for web plates of I-sections, especially those which are slenderer.

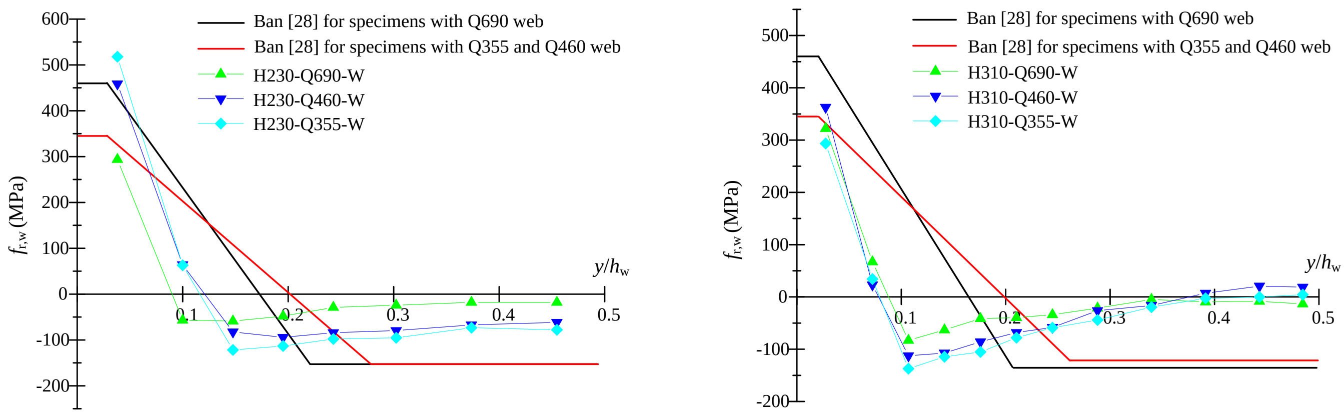

(a) "H230" specimens (b) "H310" specimens

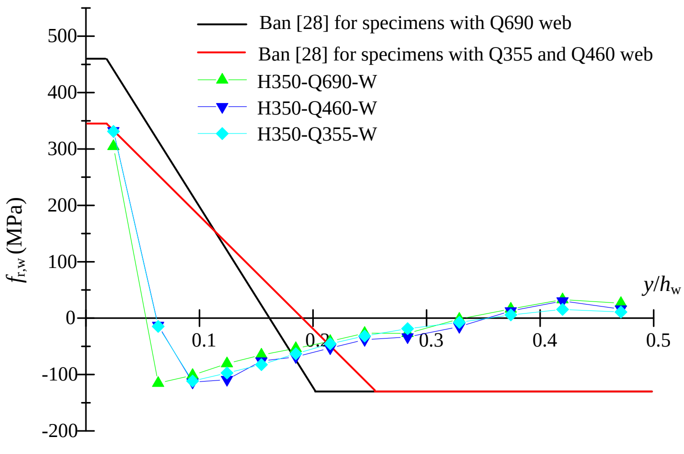

(c) "H350" specimens

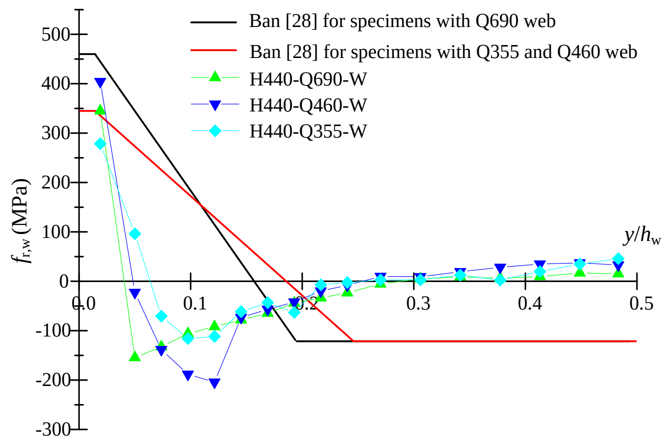

(d) "H440" specimens

Figure 19. Comparison of Ban's model and residual stress measurement results for web plates of welded I-sections

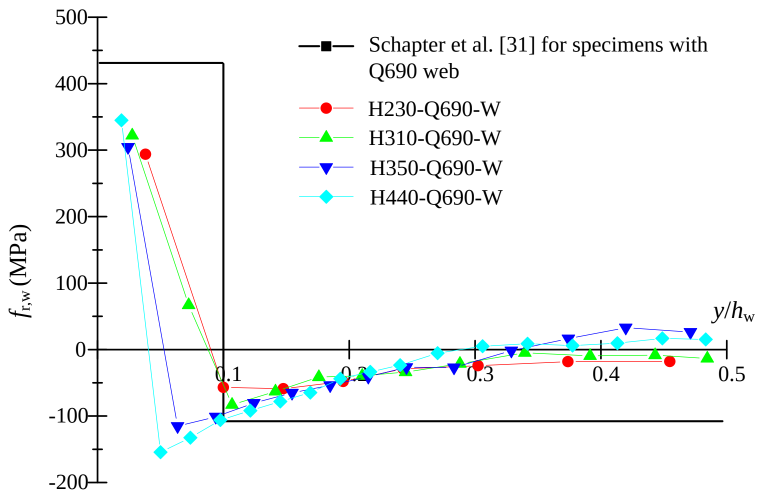

(a) "Q690" specimens

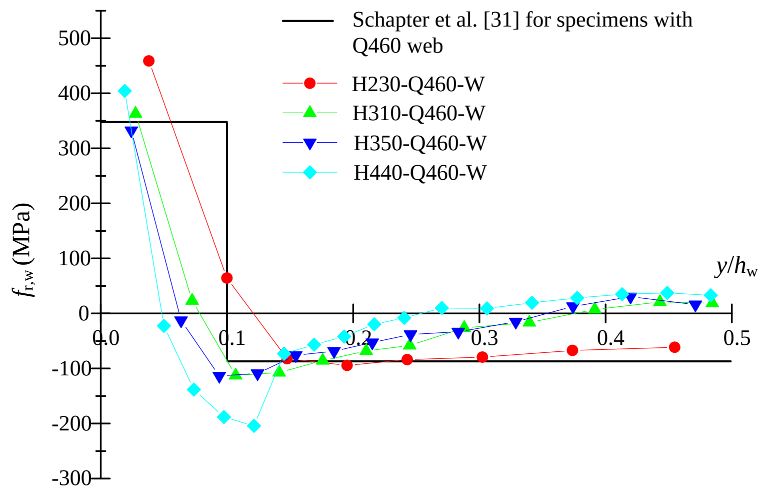

(b) "Q460" specimens

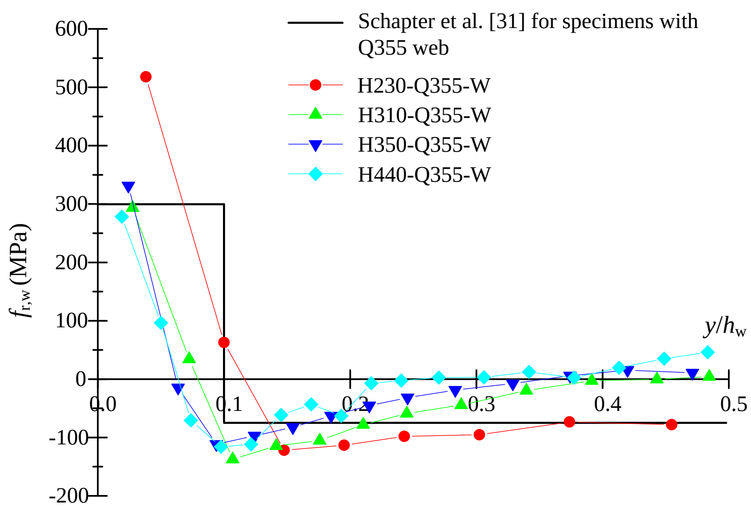

(c) “Q355” specimens

Figure 20. Comparison of Schaper’s model and residual stress measurement results for web plates of welded I-sections

4.4. Proposed model

A new residual stress distribution model is proposed for HSS and hybrid I-section test specimens investigated in this study. Based on the observations in Section 4.2, the model is divided into two groups: (1) for I-sections with web height $h_w \leqslant 210$ mm, the compressive residual stress of web is uniformly distributed (Figure 21(a)); (2) for I-sections with $h_w \geqslant 210$ mm, two segments are developed in the compression residual stresses of web, as shown in Figure 21(b). The width of tensile residual stress at the weldment of flange is selected to be the minimum value of “t_w+5h_f”and “0.25b_f”. Between them, “t_w+5h_f” is used for considering the action area of welding effect, and “0.25b_f” is to ensure the influence of welds is not overestimated for narrow flanges. The consideration of the width of tensile stress for web is similar with that of flange by using “3h_f” and “0.15h_w”. Following Ban’s model, $f_{r,ft}$, $f_{r,wt}$ and $f_{r,fte}$ are selected to be constant values: 460, 355 and 50 N/mm^2 for simplicity. Besides, the width for describing residual stress at the thermal-cut flange tips is 0.1h_f, the same as the one utilised in other models [23-24]. The other parameters, i.e., $f_{r,fc}$, $f_{r,wc}$, $b_{r,3}$, $h_{r,3}$ and $h_{r,4}$ are to be determined by self-equilbruim of the individual plate.

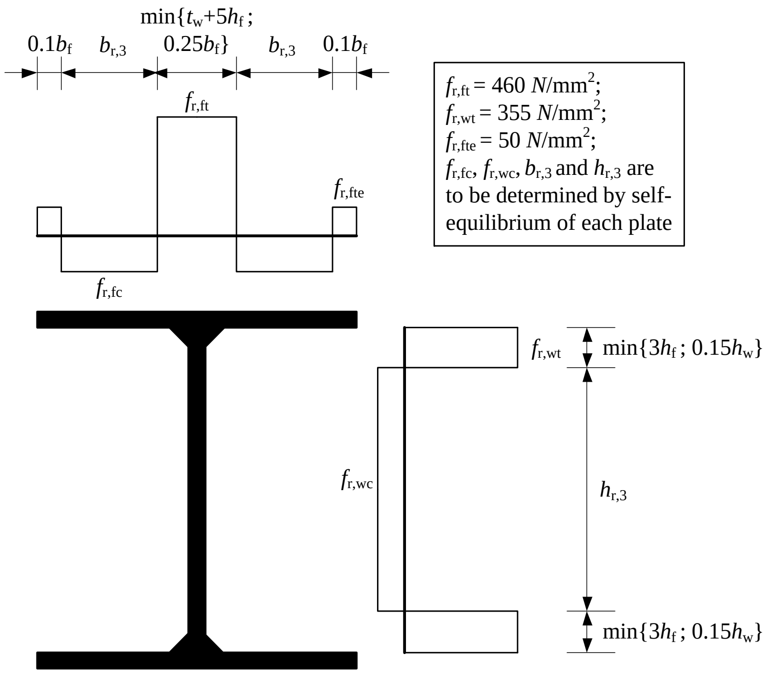

(a) for I-sections with $h_w \leq 210$mm

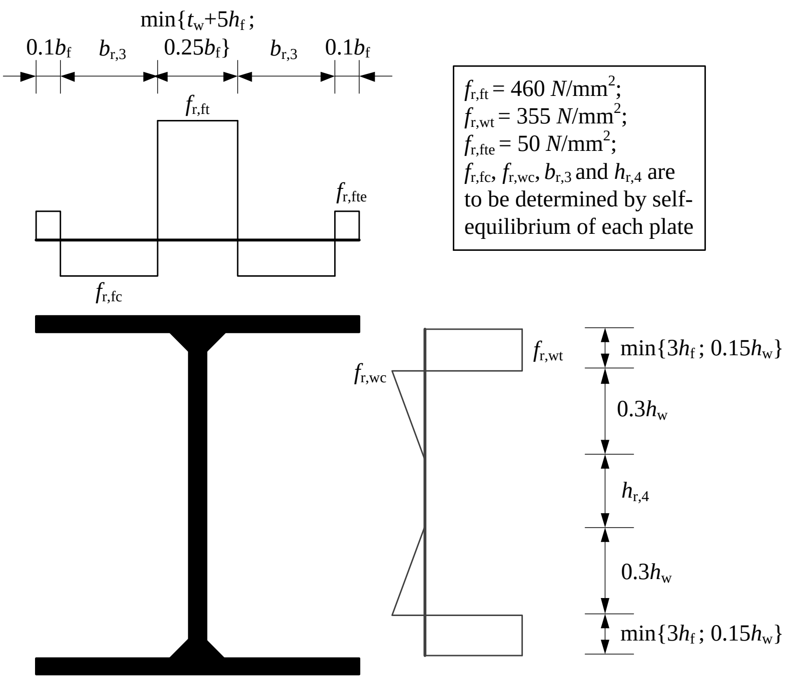

(b) for I-sections with $h_w \geq 210$ mm

Figure 21. Proposed residual stress distribution model

Note that due to the lack of specimens with h_w = 210-290 mm in this study, the selection of residual stress distribution model for these I-sections was determined from the perspective of structural design. It has been known that membrane residual stresses are always applied in finite element analysis to obtain the reasonable structural performance of components. Numerical results of “H230” and “H310” I-section models with distribution patterns (a) and (b) in Figure 21 were thus compared to seek for an appropriate model for those I-sections featured with h_w between 210 and 290 mm.

Using ABAQUS 2019, four fundamental failure modes of steel members - local buckling and flexural buckling subject to axial compression, as well as local buckling and lateral torsional buckling under pure bending were simulated. The adopted finite element models of I-sections were described in Table 6, with the corresponding boundary conditions, geometric imperfection shapes and failure modes. The measured material properties of virgin plates and the geometric imperfection magnitudes recommended in Eurocode 3 [51] were utilised in the simulations. The Length of compression members failed by local buckling and flexural buckling were selected to be $2h_w$ and $4h_w$, respectively, to prevent from the occurrence of other unanticipated failure modes. A length of 700 mm, which is greater than the limiting unbraced length L c for avoiding lateral-torsional buckling [52], was chosen to be the length of the bending members, which subject to uniform bending moments to simulate the moment span under four-point loading scenario [6, 53]. Among them, lateral constraints were provided at the mid-length section of beams expected to be failed by local buckling to ensure that their actual unbraced lengths are less than L c, as illustrated in Table 6. In addition, it can be seen from this table, each end section of members was connected to a concentric reference point (RP), where loads were applied, through rigid body constraints. In Table 6, U_X, U_Y and U_Z are the translational degrees of RP along X, Y and Z axes; R_X, R_Y and R_Z represent are the rotational degrees of RP along X, Y and Z axes.

Table 6. Finite element models used for investigating the effect of residual stress patterns

Boundary condition	Geometric imperfection shape	Failure mode
	Local buckling in compression	
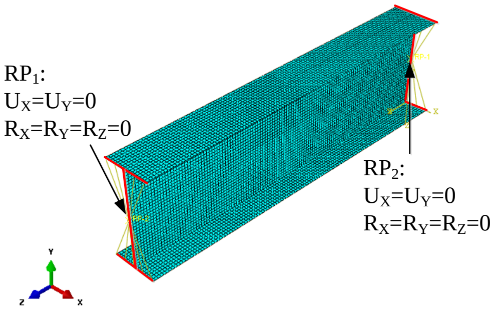	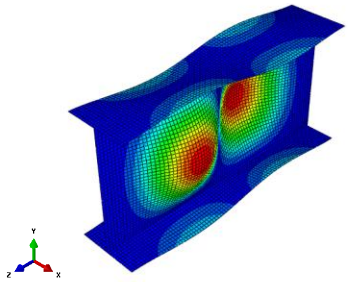	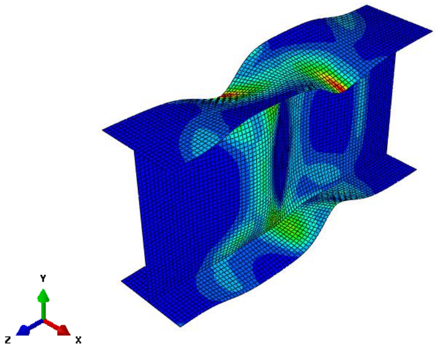
	Flexural buckling	
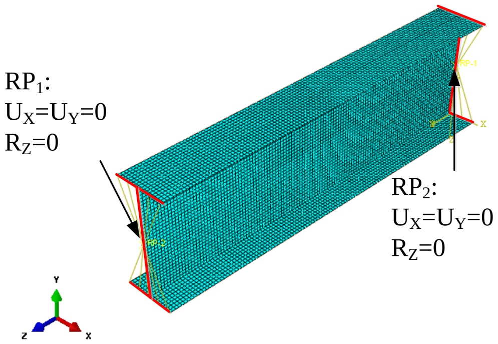	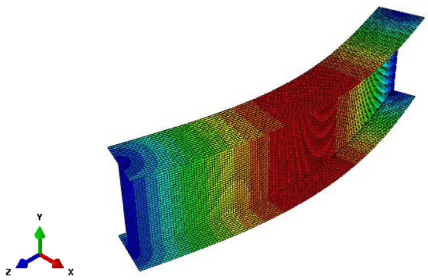	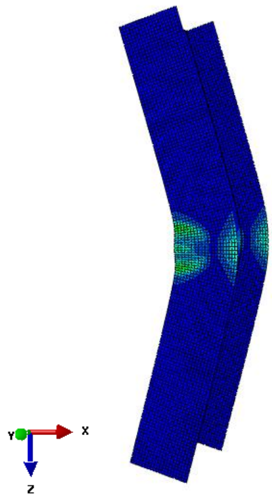
	Local buckling in bending	
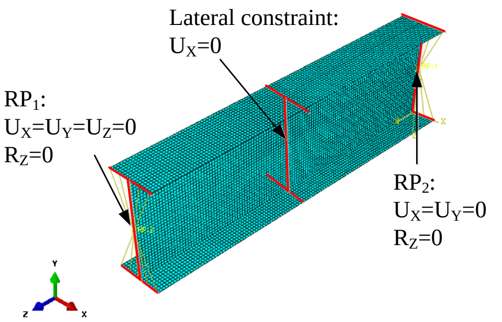	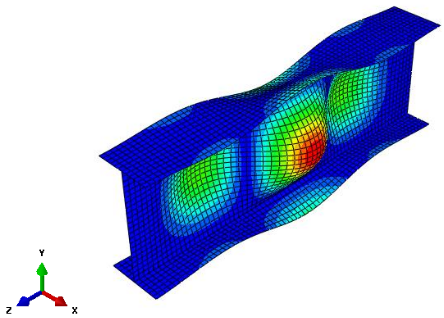	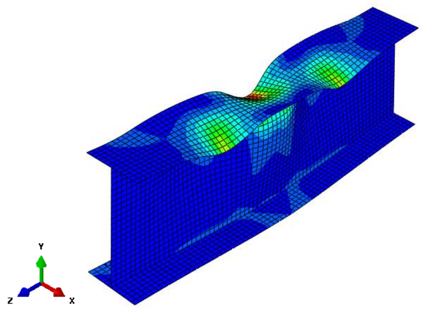
	Lateral torsional buckling	

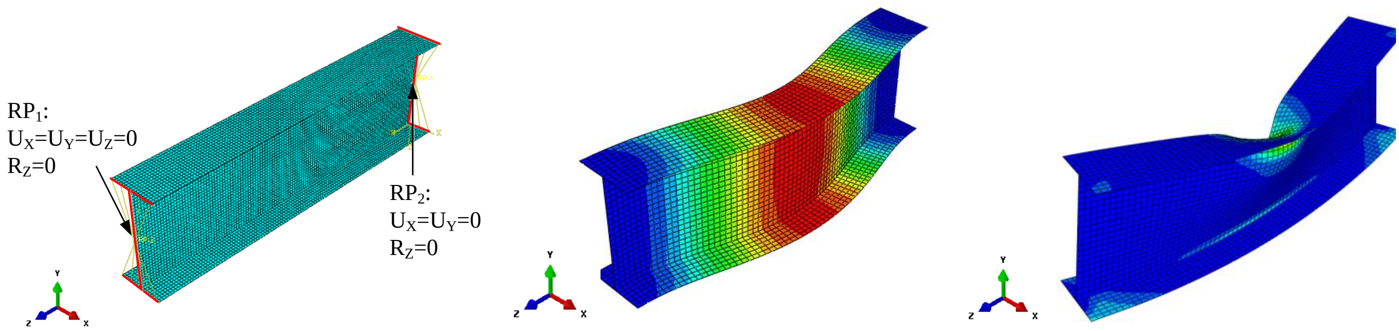

Comparison of structural performance curves for these I-sections is set out in Figure 22. In these figures, N and δ represent the axial load and end shortening of compression members; M denotes the moment resistance of flexural members. It is clear from Figure 22 that the influence of residual stress distribution patterns shown in Figure 21 is almost the same to all the mentioned structural performance for “H230” and “H310” I-section models. Structural capacities of these models were also compared, as presented in Table 7, where $F_{\text{rs-a}}$ and $F_{\text{rs-b}}$ mean the results of I-section with patterns (a) and (b), respectively. It can be seen from this table that, though the difference is fairly minor, pattern (b) generally provides safer predictions than pattern (a). As a result, pattern (b) is recommended for I-sections h_w=210-290 mm in the proposed residual stress distribution model.

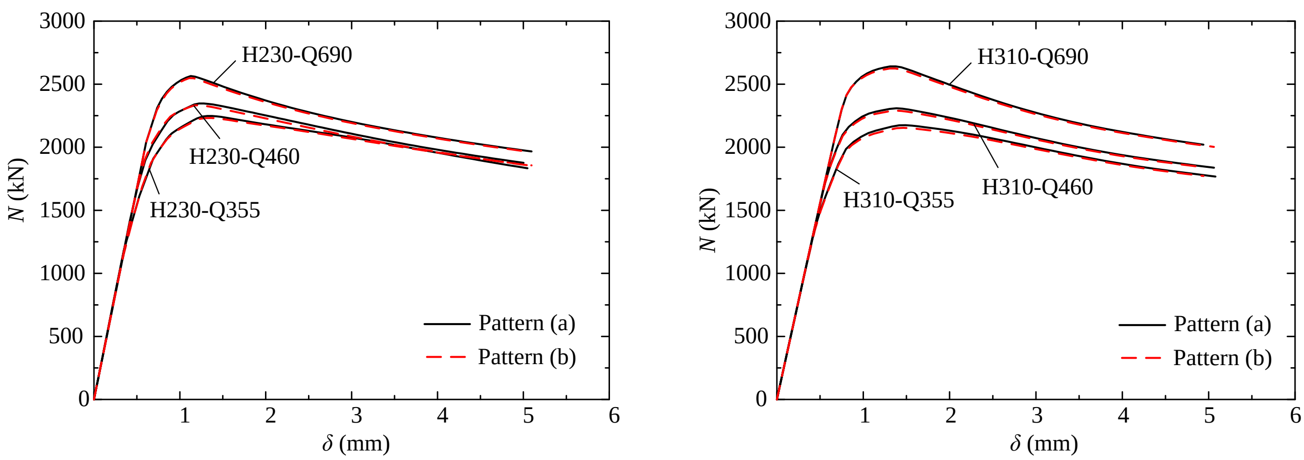

(a) Local buckling in compression

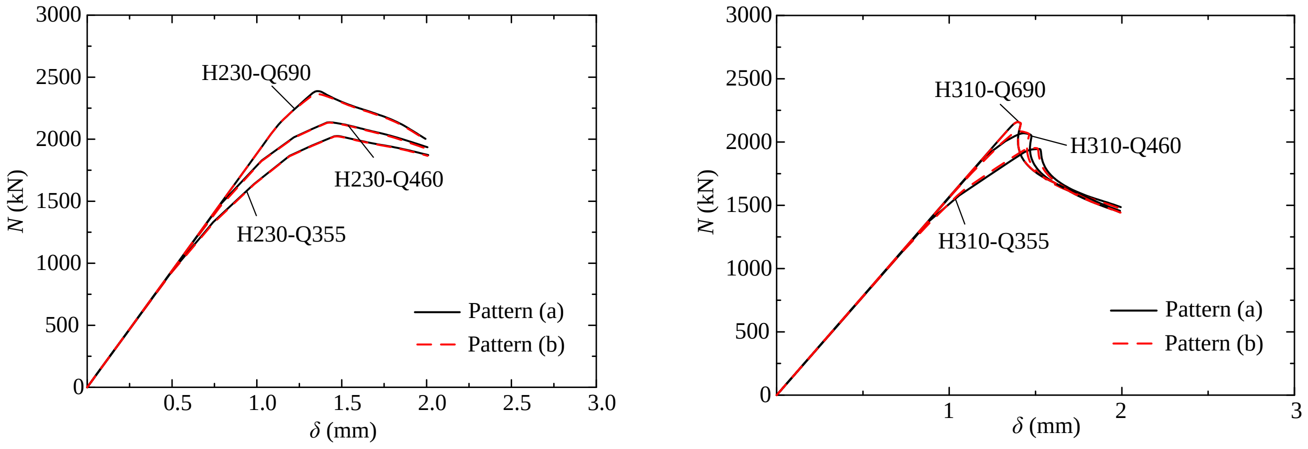

(b) Flexural buckling

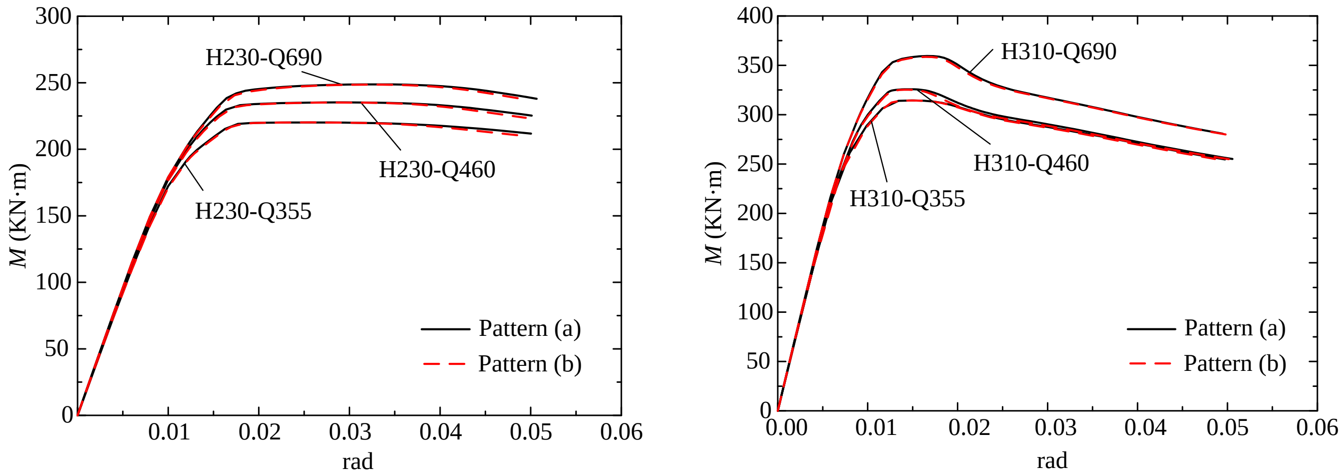

(c) Local buckling in bending

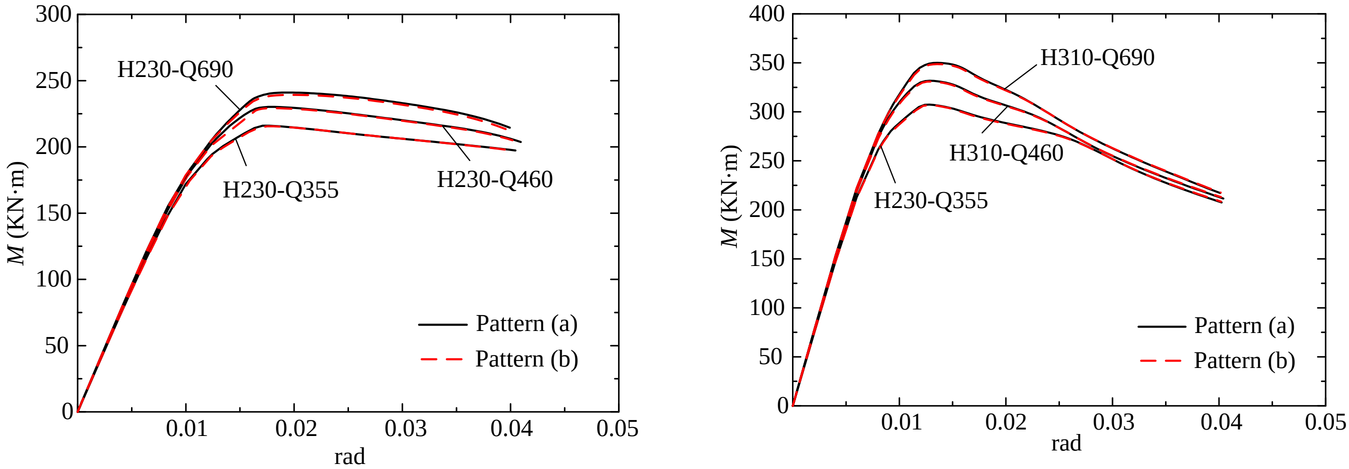

(d) Lateral torsional buckling

401 Figure 22. Comparison of structural performance curves for welded I-sections with different residual stress

402 distribution patterns

Table 7. Comparison of structural bearing capacities for welded I-sections with different residual stress distribution patterns

Structural performance	$F_{rs\text{-}b}$ / $F_{rs\text{-}a}$					
	H230-Q355	H230-Q460	H230-Q690	H310-Q355	H310-Q460	H310-Q690
Local buckling in compression	0.993	0.994	0.993	0.990	0.992	0.994
Flexural buckling	0.999	0.999	0.990	1.004	1.007	1.000
Local buckling in bending	1.000	1.000	0.999	1.000	0.998	0.997
Lateral torsional buckling	0.998	0.996	0.993	0.998	0.998	0.996

The comparison of measurement results and the proposed distribution model for flange and web plates is illustrated in Figure 23 and Figure 24, respectively. It is clear from figures that the proposed model successfully predicts the residual stress pattern of welded HSS and hybrid I-sections.

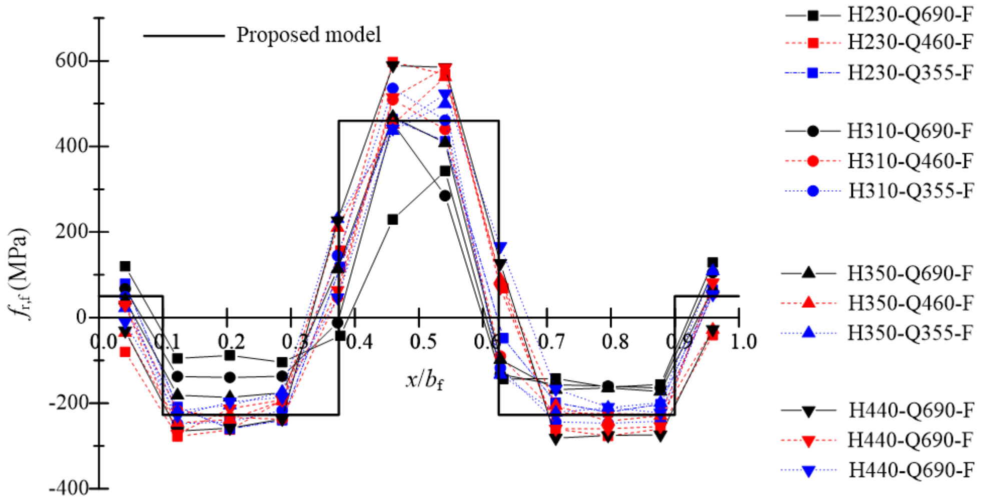

Figure 23. Comparison of the proposed model and residual stress measurement results for flange plates of I-sections

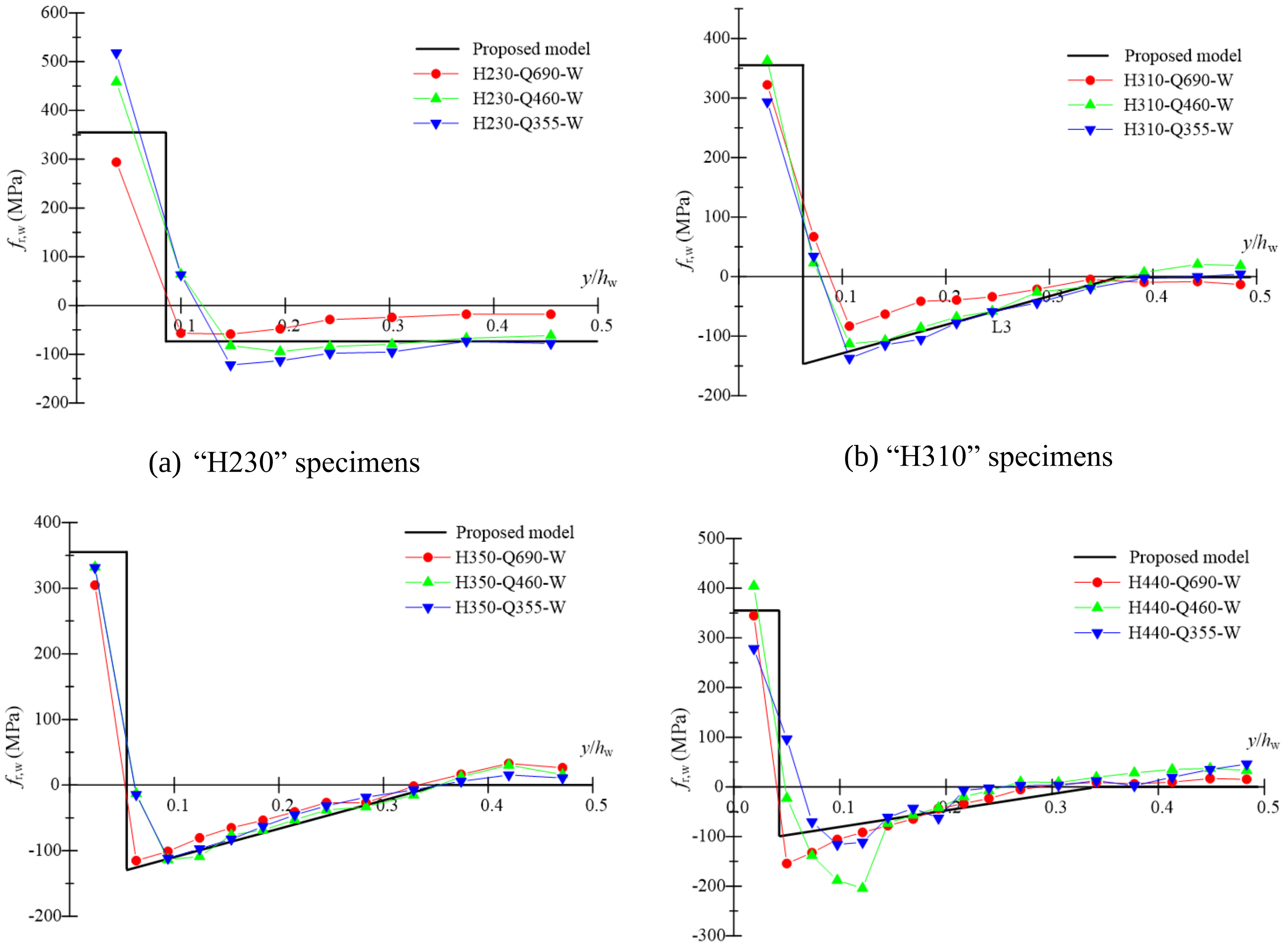

(a) "H230" specimens (b) "H310" specimens

(c) "H350" specimens (d) "H440" specimens

Figure 24. Comparison of proposed model and residual stress measurement results for web plates of I-sections

In addition, a statistical evaluation of the proposed model together with the previous predictive models in Ban [28] and Schapter et al. [31] was performed. The results of flange and web plates are in Figures 25(a) and (b). In these figures, $f_{rs,meas}$ represents the data at the measurement points; $f_{rs,model}$ means the corresponding predicted value by residual stress distribution models; μ and σ denote the mean and standard deviation based on the Normal distribution assumption.

For the flange plate, seen from Figure 25(a), the proposed model offers the closet approximation to the measured data with μ and σ of -2 MPa and 78 MPa, whilst the greatest mean value (μ = 38 MPa) and deviation (σ = 140 MPa) of $f_{rs,meas}$-$f_{rs,model}$ are given by Ban's model and Schapter's model, respectively. As shown in Figure 25(b), for the web plate, the least scattered predictive accuracy is provided by the proposed model with σ of 78 MPa, which is much less than those of previous models -173 MPa and 155 MPa. Also, it is obvious from this figure, most data points of $f_{rs,meas}$ - $f_{rs,model}$ from the proposed model were found to be concentrated between -50 MPa and 50 MPa, confirming the effectiveness of the proposed model for welded HSS and hybrid I-sections.

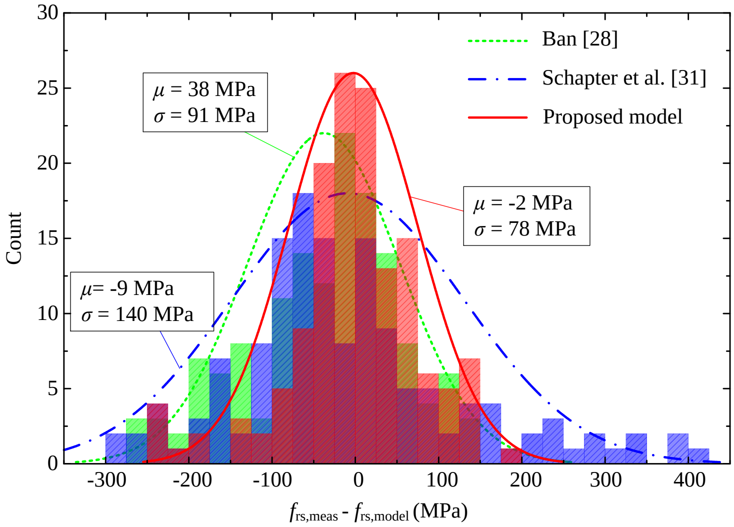

(a) Flange

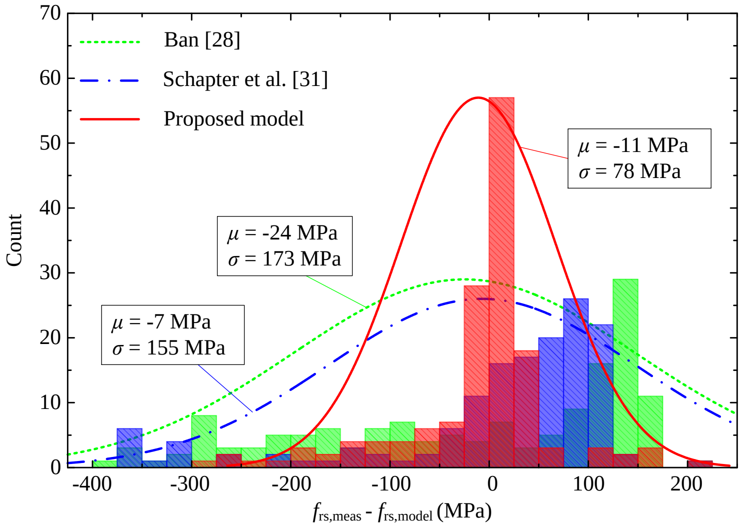

(b) Web

Figure 25. Evaluation of residual stress distribution models based on the measurement data

5. Conclusion

The research examines the welding effect on the material properties and residual stresses of welded high strength steel (HSS) and hybrid I-sections. Covering three material combinations and four web slenderness, a total of twelve I-section test specimens were investigated. Tensile tests of coupons cut from both virgin plates and welded I-sections were carried out, followed by a metallographic analysis of welding position. It has shown that the welding effect on the mechanical behaviour of steel materials varies depending on the chemical composition and microstructure. The welding possess was found to increase the yield strength of the low bainite low carbon steel Q460 because of the precipitation strengthening from micro-alloying.

Moreover, residual stress measurement for HSS and hybrid I-sections was conducted. The measurement results revealed that the residual stress distribution of I-sections is independent with the steel strength grade of constitutive plates. It was also concluded that for I-sections with web height less than 210 mm, the compressive stress of the web is uniformly distributed, while gradually decreased compressive residual stresses were detected for specimens with web height greater than 210 mm. A new residual stress distribution model for welded HSS and hybrid I-sections tested in this study was proposed.

CRediT authorship contribution statement

Shuxian Chen: Investigation, Writing – original draft. Jun-zhi Liu: Writing – review & editing. Tak-Ming Chan: Writing – review & editing, Supervision, Funding acquisition.

Declaration of competing interest

The authors declare that they have no known competing financial and personal relationships with other people or organizations that could inappropriately influence this work.

Acknowledgements

The funding support from the Chinese National Engineering Research Centre for Steel Construction (Hong Kong Branch) at The Hong Kong Polytechnic University is gratefully acknowledged. The authors sincerely appreciate the technical supports from Dr. M.P. Ho, Mr. H.C. Leung, Mr. P. W. Shum and Mr. C.H. Tang in the Industrial Centre, Mr. H.Y. Leung of the Mechanical Workshop at The Hong Kong Polytechnic University. Heartfelt thanks are given to Mr. Y.C. Wang and Ms. Y.T. Xiao in the Chinese National Engineering Research Centre for Steel Construction (Hong Kong Branch) for their academic advice on the metallographic analysis.

Reference

[1] Wilson, W. (1944) Physical properties that affect behaviour of structural members. Transactions of the American Society of Civil Engineers. 109 (1), 279-289.

[2] Ito, M. Nozaka, K., Shirosaki, T. and Yamasaki, K. (2005) Experimental study on moment-plastic rotation capacity of hybrid beams. Journal of Bridge Engineering. 10 (4), 490-496.

[3] Wang, C. S., Duan, L., Chen, Y. F. and Wang, S. C. (2016) Flexural behaviour and ductility of hybrid high performance steel I-girders. Journal of Constructional Steel Research. 125, 1-14.

[4] Bartsch, H., Eyben, F., Pauli, G., Schaffrath, S. and Feldmann, M. (2021) Experimental and numerical investigations on the rotation capacity of high-strength steel beams. Journal of Structural Engineering. 147(6), 04021067.

[5] Lee, C.H., Han, K.H., Uang, C.M., Kim, D.K., Park, C.H. and Kim, J.H. (2013) Flexural strength and rotation capacity of I-shaped beams fabricated from 800-MPa steel. Journal of Structural Engineering. 139(6), 1043-1058.

[6] Chen, S.X., Fang, H. Liu, J.Z. and Chan, T.M. (2022) Design for local buckling behaviour of welded

high strength steel I-sections under bending. Thin-Walled Structures. 172, 108792.

[7] Liu, J.Z., Fang, H., Chen, S.X. and Chan, T.M. (2022) Material properties and residual stresses of high strength steel hexagonal hollow sections. Journal of Constructional Steel Research. 190, 107061.

[8] Singh, R. (2012) Applied Welding Engineering: Processes, Codes and Standards, 2nd edition. Oxford, Butterworth-Heinemann, Elsevier.

[9] Javidan, F., Heidarpour, A., Zhao, X. L., Hutchinson, C.R. and Minkkinen, J. (2016) Effect of weld on the mechanical properties of high strength and ultra-high strength steel tubes in fabricated hybrid sections. Engineering Structures. 118,16–27.

[10] Hai, L.T., Sun, F.F., Zhao, C., Li, G.Q., Wang, Y.B. (2018) Experimental cyclic behavior and constitutive modeling of high strength structural steels. Construction and Building Materials. 189, 1264–1285.

[11] Ho, H.C., Liu, X., Chung, K.F., Elghazouli, A.Y., and Xiao, M. (2018) Hysteretic behaviour of high strength S690 steel materials under low cycle high strain tests. Engineering Structures. 165, 222–236.

[12] Ho, H.C., Chung, K.F., Liu, X., Xiao, M., Nethercot, D.A. (2019) Modelling tensile tests on high strength S690 steel materials undergoing large deformations. Engineering Structures. 192,305–322.

[13] Ho, H.C., Xiao, M., Hu, Y.F., Guo, Y.B., Chung, K.F., Yama, M.C.H., Nethercot, D.A. (2020) Determination of a full range constitutive model for high strength S690 steels. Journal of Constructional Steel Research. 174, 106275.

[14] Zhang, C.T., Wang, R.H., Song, G.B. (2020) Effects of pre-fatigue damage on mechanical properties of Q690 high strength steel. Construction and Building Materials. 252,118845.

[15] Cadoni E., and Forni, D. (2020) Strain-rate effects on S690QL high strength steel under tensile loading. Journal of Constructional Steel Research. 175, 106348.

[16] Chung, K.F., Ho, H.C., Hu, Y.F., Wang, K., Liu, X., Xiao, M., Nethercot, D.A. (2020) Experimental

evidence on structural adequacy of high strength S690 steel welded joints with different heat input energy. Engineering Structures. 204,110051.

[17] Fang, H., Chan, T.M., and Young, B. (2018) Material properties and residual stresses of octagonal high strength steel hollow sections. Journal of Constructional Steel Research. 148, 479–490.

[18] Chen, J. B., Liu, H.X. and Chan, T.M. (2020) Material properties and residual stresses of cold-formed octagonal sections. Journal of Constructional Steel Research. 170, 106078.

[19] Chen, J.B., and Chan, T.M. (2020) Material properties and residual stresses of cold-formed high-strength-steel circular hollow sections. Journal of Constructional Steel Research. 170,106099.

[20] Kang, L., Wang, Y.Q., Liu, X. P. and Uy, B (2019) Investigation of residual stresses of hybrid normal and high strength steel (HNHSS) welded box sections. Steel and Composite Structures. 33(4), 489-507.

[21] Wang, Y.B., Li, G.Q. and Chen, S.W. (2012) Residual stresses in welded flame-cut high strength steel H-sections. Journal of Constructional Steel Research.79,159–165.

[22] Li, T.J., Li, G. Q. and Wang, Y.B. (2015) Residual stress tests of welded Q690 high-strength steel box- and H-sections. Journal of Constructional Steel Research. 115, 283–289.

[23] Yang, B. Nie, S.D., Xiong, G., et al. (2016) Residual stresses in welded I-shaped sections fabricated from Q460GJ structural steel plates. Journal of Constructional Steel Research. 122, 261–273.

[24] Yang, B., Zhu, Q., Nie, S.D., Elchalakani, M., Xiong, G. (2018) Experimental and model investigation on residual stresses in Q460GJ thick-walled I-shaped sections. Journal of Constructional Steel Research. 145, 489–503.

[25] Liu, X. (2017) Structural Effects of Welding onto High Strength S690 Steel Plates and Welded Sections. Ph.D. Thesis. The Hong Kong Polytechnic University, Hong Kong.

[26] Liu, X. and Chung, K.F. (2018) Experimental and numerical investigation into temperature histories and residual stress distributions of high strength steel S690 welded H-sections. Engineering Structures. 165,

396-411.

[27] Li, D.X., Paradowska, A., Uy, B., Wang, J., Khana, M. (2020) Residual stresses of box and I-shaped columns fabricated from S960 ultra-high-strength steel. Journal of Constructional Steel Research. 166,105904.

[28] Ban, H.Y. (2012) Research on the Overall Buckling Behavior and Design Method of High Strength Steel Columns under Axial Compression. Ph.D. Thesis. Tsinghua University, Beijing. (in Chinese)

[29] Frost, R. and Schilling, C. (1964) Behaviour of hybrid beams subjected to static loads. Journal of the Structural Division, ASCE. 90 (ST3), 55–86.

[30] Nagarajarao, N. R., Marek, P. and Tall, L. (1972) Welded hybrid steel columns. Welding research supplement, 462-472.

[31] Schaper, L., Tankova, T., Silva, L. Sim˜oes da and Knobloch, M. (2022) A novel residual stress model for welded I-sections. Journal of Constructional Steel Research. 188, 107017.

[32] Code for design of steel structures committee (2003) Application Construal of Code for Design of Steel Structures in China. Planning Press, Beijing, China. (in Chinese).

[33] European Convention for Constructional Steelwork (ECCS) (1984) Technical Committee 8: Ultimate Limit State Calculation of Sway Frames with Rigid Joints, ECCS Publication No.33, Brussels, Belgium.

[34] CEN/TC250 (2021) Eurocode 3: Design of steel structures - Part 1–14: Design assisted by finite element analysis, CEN/TC 250/SC 3 N 3296 - prEN 1993–1-14 – Draft version.

[35] Mvola, B., Kah, P., Martikainen, J. and Suoranta, R. (2016) Dissimilar high-strength steels: fusion welded joints, mismatches, and challenges. Reviews on Advanced Materials Science. 44, 46-159.

[36] Bayock, F.N., Kah, P., Mvola, B. and P, Layus (2019) Experimental review of thermal analysis of dissimilar welds of high-Strength Steel. Reviews on Advanced Materials Science. 58, 38–49.

[37] Standardization Administration of the P.R.C. (2008) GB/T 8110-2008 Welding electrodes and rods for

gas shielding arc welding of carbon and low alloy steel. Beijing, Standardization Administration of the P.R.C. (in Chinese)

[38] International Organization for Standardization (2019) ISO 6892-1:2019. Metallic materials-Tensile testing-Part 1: Method of test at room temperature. Genève, ISO.

[39] Njock Bayock, F. (2020) Thermal Analysis of Dissimilar Weld Joints of High-Strength and Ultra-High-Strength Steels. Ph.D. Thesis. Lappeenranta-Lahti University of Technology LUT, Lappeenranta, Finland.

[40] Li, X.B. (2011) Effect of Tempering Process on Microstructures and Mechanical Properties of Low-Carbon High Strength Bainitic Steel. Master Thesis, Northeastern University, Shenyang, China. (in Chinese)

[41] Zhou, Y.L., Jia, T., Zhang, X.J., Liu, Z.Y., Misra, R.D.K. (2015) Investigation on tempering of granular bainite in an offshore platform steel. Materials Science & Engineering A. 626, 352-361.

[42] Zhu, M., Xu, G., Zhou, M.X., Yuan, Q., Tian, J.Y. and Hu, H.J. (2018) Effects of tempering on the microstructure and properties of a high-strength bainite rail steel with good toughness. Metals. 8(7), 484.

[43] Feng, R., Li, S.L., Li, Z.S., Tian, L. (2012) Variations of microstructure and properties of 690 MPa grade low carbon bainitic steel after tempering. Materials Science & Engineering A. 558, 205–210.

[44] He, M.T. (2019) Development of Q690D Plate High Strength Steel for Construction Machinery. Northeastern University. Master thesis. Shenyang, China (in Chinese)

[45] Cruise, R.B., Gardner, L. (2008) Residual stress analysis of structural stainless steel sections. Journal of Constructional Steel Research. 64, 352–366.

[46] Huang, Y. and Young, B. (2012) Material properties of cold-formed lean duplex stainless steel sections. Thin-Walled Structures. 54,72–81.

[47] Chen, M.T. and Young, Ben (2019) Material properties and structural behavior of cold-formed steel elliptical hollow section stub columns. Thin-Walled Structures.134, 111–126.

[48] Hu, Y.F., Chung, K.F., Ban, H.Y., Nethercot, D.A. (2020) Investigations into residual stresses in S690 cold-formed circular hollow sections due to transverse bending and longitudinal welding. Engineering Structures. 219,110911.

[49] Xiao, M., Hu, Y.F., Jin, H., Chung, K.F., Nethercot. D. A. (2022) Prediction of residual stresses in high-strength S690 cold-formed square hollow sections using integrated numerical simulations. Engineering Structures. 253,113682

[50] Nemchinsky, V.A. and Severance, W. S. (2006) What we know and what we do not know about plasma arc cutting. Journal of Physics D: Applied Physics. 39, 423–438.

[51] European Committee for Standardization. EN 1993-1-5:2006. Eurocode 3 - Design of Steel Structures - Part 1-5: Plated Structural Elements. Brussels: CEN.; 2006.

[52] European Committee for Standardization. EN 1993-1-1:2005. Eurocode 3 - Design of Steel Structures - Part 1-1: General rules and rules for buildings. Brussels: CEN.; 2005.

[53] Ma, J.L., Chan, T.M., Young, B. (2017) Design of cold-formed high strength steel tubular beams. Engineering Structures. 151, 432–443.